Monthly Notices of the ROYAL ASTRONOMICAL SOCIETY

MNRAS **517,** 3804–3821 (2022) https://doi.org/10.1093/mnras/stac2154
Advance Access publication 2022 August 4

# Towards a better understanding of ice mantle desorption by cosmic rays

Jonathan M. C. Rawlings ★

*Department of Physics and Astronomy, University College London, Gower Street, London WC1E 6BT, UK*

Accepted 2022 July 28. Received 2022 July 28; in original form 2022 March 13

## ABSTRACT

The standard model of cosmic ray heating-induced desorption of interstellar ices is based on a continuous representation of the sporadic desorption of ice mantle components from classical (0.1 μm) dust grains. This has been re-evaluated and developed to include tracking the desorption through (extended) grain cooling profiles, consideration of grain size-dependencies and constraints to the efficiencies. A model was then constructed to study the true, sporadic, nature of the process with possible allowances from species co-desorption and whole mantle desorption from very small grains. The key results from the study are that the desorption rates are highly uncertain, but almost certainly significantly larger than have been previously determined. For typical interstellar grain size distributions it is found that the desorption is dominated by the contributions from the smallest grains. The sporadic desorption model shows that, if the interval between cosmic ray impacts is comparable to, or less than, the freeze-out time-scale, the continuous representation is inapplicable; chemical changes may occur on very long time-scales, resulting in strong gas phase chemical enrichments that have very non-linear dependences on the cosmic ray flux. The inclusion of even limited levels of species co-desorption and/or the contribution from very small grains further enhances the rates, especially for species such as $H_2O$. In general, we find that cosmic ray heating is the dominant desorption mechanism in dark environments. These results may have important chemical implications for protostellar and protoplanetary environments.

**Key words:** astrochemistry – molecular processes – cosmic rays – dust, extinction – ISM: molecules.

## 1 INTRODUCTION

In the dense, cold, environments of molecular clouds the, often very rich, chemistry is determined by both gas-phase and solid-state reactions. These are interconnected by the freeze-out of gas-phase species and the sublimation, or desorption, of solid-state species.

In dense gas with a cold dust component, freeze-out is very rapid (and typically faster than the time-scale for dynamical evolution), so that the desorption processes are required to explain the observed abundances of gas-phase species (e.g. Tafalla et al. 2004; Caselli et al. 2012). Indeed, the observed presence of tightly bound complex organic molecules (e.g. Cernicharo et al. 2012) is indicative of the presence not just of efficient desorption, but also of energetic processes that drive the chemistry of their formation.

Obviously, to understand the chemical composition and evolution of a molecular cloud or star-forming region, it is essential to have an accurate understanding of the desorption processes. A variety of mechanisms have been proposed but, broadly speaking, these can be divided into continuous processes, and sporadic processes (Roberts et al. 2007). Examples of the former include thermal desorption (Watson 1976), photodesorption (direct and cosmic ray induced) – often driven by the photodissociation of molecules in the surface layers of ice mantles, and desorption that is driven by the enthalpy of molecule formation in the solid-state (e.g. Minissale et al. 2016). Examples of the latter include ice mantle 'explosions' following the release of trapped chemical energy (e.g. Cecchi–Pestellini et al. 2010) and desorption driven by the impact and passage of cosmic ray particles through a grain (e.g. Léger, Jura & Omont 1985; Hasegawa & Herbst 1993; Bringa & Johnson 2004; Herbst & Cuppen 2006).

In recent years considerable attention has been paid to photodesorption processes, which may operate dissociatively (e.g. for $H_2O$) or non-dissociatively (e.g. for CO) in the surface layers of ice mantles (e.g. Öberg et al. 2009; Öberg, van Dishoeck & Linnartz 2009). Such processes, which typically have a yield of $\sim 10^{-3}$, are believed to be particularly important in regions of intermediate extinction ($A_v \sim 1 - 10$) due to direct photodesorption by the attenuated interstellar radiation field, but also in regions of higher extinction, where the UV radiation field is dominated by the indirect cosmic ray excitation of $H_2$ Lyman and Werner bands (Prasad & Tarafdar 1983). Indeed, photodesorption is often taken to be the dominant desorption process in cold, dense environments. It has been suggested that this may even be true in very high density, dark cores (Caselli et al. 2012).

Desorption can also be effected as a result of impulsive heating by (heavy ion) cosmic ray particles as they pass through grains. However, whilst photodesorption has been very well studied, both theoretically and in the laboratory, the same cannot be said for cosmic ray induced desorption and the effective rates that have been determined for this process are almost entirely theoretical.

In the standard representation, which we describe in the following section, the mechanism is one of sporadic heating by cosmic ray impact events, leading to grain heating and the rapid thermal desorption/sublimation of ice mantle species. These impacts are rare (typically occuring once every Myr) but they promote very efficient, possibly even catastrophic, desorption so that the net effect

★ E-mail: jcr@star.ucl.ac.uk

on the chemical abundances (particularly of gas-phase species) may be highly significant.

In this paper, we argue that – even within the commonly adopted paradigm in which cosmic ray induced desorption is represented by a continuous process – following periodic whole grain heating/desorption by cosmic rays of a single type and energy – the rates have been severely underestimated. There are a variety of reasons for this; including an underestimation of the grain cooling/ice evaporation time-scale, a lack of consideration of ice species co-desorption and the effects of consideration of varying grain sizes and cosmic ray properties/energies. The last of these has been considered in recent publications (see Section 7 below) and we do not discuss it in this study. However, the other issues have not been considered comprehensively, nor has the effect of simplifying the sporadic grain heating to a continuous desorption process. Once these factors have been included we find that, for most species of astrochemical interest, cosmic ray-induced desorption is almost certainly the dominant desorption mechanism in the denser, darker parts of star-forming regions, but remains very poorly constrained.

The structure of the paper is as follows: In Section 2, we give an outline of the physical processes that are involved in cosmic ray induced desorption and describe the continuous desorption representation that is widely adopted in astrochemical models. The extension of this model to more realistic grain size distributions is explained in Section 3, whilst in Section 4 we consider the limitations of that model, and their implications, as well as the possible major contribution to the process that is made by very small grains. In Section 5, we describe a model that includes the sporadic nature of the desorption events, as well as the possibility of ice species co-desorption, and the results from that model are presented and discussed in Section 6. Section 7 compares our findings to other, recent, studies and a summary of our findings and the conclusions are given in section 8.

## 2 COSMIC-RAY INDUCED DESORPTION

The physics of the interaction between a cosmic ray particle (typically, a high energy massive ion) and an ice-coated grain is complex. In the context of how that interaction effects ice mantle sublimation or desorption the process is often (over-)simplified as being represented by the sporadic heating of the whole grain. The resulting desorption that is driven by the heating of grains and the sublimation of ices is very poorly understood/quantified.

In fact, the interaction between a cosmic ray and an icy grain has several physical stages (Bringa & Johnson 2004): as the particle passes through a grain it causes excitations, ionizations, and deposits energy within an approximate cylinder of interaction, with a typical radius of $\sim$100 Å. The instantaneous effects of this interaction are initially manifest at the areas on the surface of the grain where the cosmic ray particle enters and exits, the so-called 'hotspots', and spread to the rest of the grain as a result of thermal diffusion. The nature and physics of this interaction is empirically ill-defined, but molecular dynamics simulations suggest that the physical processes can be divided into four phases: (i) initial excitations and primary/secondary ionizations. It has been estimated that as much as 40 per cent of the impact energy could be carried away by fast electrons (Léger et al. 1985), (ii) relaxation/recombinations, leading to prompt desorption of hot atoms from the 'hotspots', possibly leading to a heat-spike pressure pulse capable of significant energy transfer, (iii) localized thermal diffusion and evaporation – 'thermal spike sputtering' and then, finally, (iv) thermal diffusion throughout the grain – 'whole grain heating' (WGH) and evaporative cooling. The relative importance of the different phases (and the resulting desorption of the ices) will depend on a number of factors. So, for example, it is obvious that if the grain size is comparable to the width of the interaction cylinder then the distinction between these processes becomes very unclear.

Most studies of cosmic ray driven desorption are predicated on the assumption that the deposition of energy following a cosmic ray impact leads either to 'hotspot' heating or, more usually, whole grain heating that dominates the desorption process due to thermal evaporation (e.g. Hasegawa & Herbst 1993) or else through the triggered release of trapped chemical energy in exothermic reactions (d'Hendecourt et al. 1982; Léger et al. 1985; Schutte & Greengerg 1991; Rawlings et al. 2013) leading to total sublimation in ice mantle 'explosions'. In addition to promoting efficient ice desorption, cosmic ray-induced reactions in the ices between supra-thermal dissociation products may drive the efficient formation of complex organic molecules (COMs; Shingledecker et al. 2018) and the heating process may also enable the efficient diffusion of solid-state species, driving a vigorous surface chemistry (Kalvāns 2016).

The astrochemical significance of cosmic ray induced desorption was described in the seminal study of Léger et al. (1985) in the context of a model in which the energy deposition by the passage of a cosmic ray particle, or an X-ray photon, through a grain effects thermal desorption of ice mantle species, or else triggers the release of trapped chemical energy in an ice mantle 'explosion'. The calculations included the effects of both whole grain heating and spot heating, the latter being particularly important for the larger grains. To assess the possible importance of chemical explosions, the study paid particular attention to heating events that are capable of yielding $T_{\rm peak} > 27$ K, this being the nominal temperature threshold to enable the mobility of radicals and trigger a chemical explosion (d'Hendecourt et al. 1982).

Despite the fact that such cosmic ray impacts are infrequent (typically one per Myr, when considering 'classical' grains of radius 0.1 μm) the effects on the chemistry were found to be significant. In their model, Léger et al. (1985) considered iron nuclei impacting olivine grains, although this has been extended in subsequent studies to consider different grain compositions and a wider range of cosmic ray types and energies (e.g. Shen et al. 2004).

### 2.1 The continuous desorption representation

The process described above is sporadic, with long intervals between impact events. This is not particularly easy to incorporate into astrochemical models, the subject of which may be environments in which the physical conditions are evolving on comparable, or shorter, time-scales.

In order to provide an easily applicable analytical implementation, appropriate for models of time-dependent chemistries, Hasegawa & Herbst (1993) – hereafter HH93, formulated a continuous representation of the desorption process, and this has become the standard model that has been adopted in most subsequent astrochemical studies. As indicated above, the mechanism involves the raising of the grain temperature to a level such that the ices can sublimate. The efficiency of the process thus depends on the binding energies of the various ice species and the energy and impact rate of the cosmic rays.

As well as the representation of the sporadic process by continuous desorption, the HH93 representation is based on the following three important simplifications: (i) the desorption process is entirely dominated by whole grain heating/evaporation, (ii) the grain size distribution for the interstellar dust particles can be represented by a single 'classical' grain size value of $a = 0.1$ μm, and (iii) the

cosmic ray spectrum can be represented by a single (average) energy deposition of $\Delta E \sim 0.4$ MeV occurring (on average) at intervals of $t_{\rm impact} \sim 1$ Myr (for a 0.1-μm grain) corresponding to impacts by relativistic Fe nuclei with energies in the range 20–70 Mev. The energy deposition is proportional to the path-length through the grain (Léger et al. 1985; Bringa & Johnson 2004), so that this implies a mean 'stopping power' of 20 Gev cm$^{-1}$. With these parameters, HH93 determined that, the temperature of the grain would be raised to a peak value of $T_{\rm peak} \sim 70$ K, assuming WGH.

The grains then cool by evaporative cooling, caused by desorption of ice species (effectively releasing an energy greater than or equal to the local binding energy of each ejected molecule). For the grain size and temperature under consideration this is more efficient than radiative cooling and occurs on a very short time-scale ($\sim 10^{-5}$ s$^{-1}$), eventually quenching the desorption. Rather than follow the desorption through any one heating/cooling event, the simplification is made that the desorption all occurs at $T = T_{\rm peak}$ for a nominal cooling time ($t_{\rm cool}$); noting that thermal desorption is strongly temperature-dependent. The cycle is then repeated. For $T_{\rm peak} = 70$ K, thermal desorption is only significant for the more weakly bound (volatile) species, such as CO and $CH_4$ and it is important to try and quantify the desorption efficiency as accurately as possible when modelling the chemistry of these species.

This, of course, is only strictly applicable to ices whose composition is dominated by volatile species and is based on a number of important additional assumptions including: (iv) the requirement that there are sufficient volatile molecules in the top layer of the ice to enable evaporative cooling, (v) that the inferred continuous desorption rate for any species does not imply a net loss in any one cooling cycle that exceeds the available budget of molecules in the ice, and (vi) that a single binding energy can be used to describe the cooling throughout the evaporation process etc. The model is therefore predicated on the assumption that one (volatile) species is the overwhelmingly dominant component of the (surface layers) of the ice mantles so that it is (a) the principal sublimate, and (b) the dominant (evaporative) coolant. In HH93, this species is taken to be CO, and these assumptions are probably satisfied in regions that are very cold, dense and where advanced freeze-out has occurred. However the validity of these, and the other assumptions, is discussed below.

To represent the episodic process as a continuous desorption rate, $k_{\rm crd}^{\rm CO}$ (per bound molecule, per second) the thermal evaporation rate (at $T = T_{\rm peak} = 70$ K) is then multiplied by the 'duty cycle', equal to the cooling time-scale ($t_{\rm cool}$) divided by the average interval between cosmic ray impacts ($t_{\rm impact}$):

$$k_{\rm crd}^{\rm CO} = k_{\rm evap}^{\rm CO}.\left[\frac{t_{\rm cool}}{t_{\rm impact}}\right].$$

The rate of thermal sublimation (per molecule) for a zeroth-order process is given by

$$k_{\rm evap}^{\rm i} = \nu_0^{\rm i} e^{-E_{\rm B}^{\rm i}/kT_{\rm dust}}\ {\rm s}^{-1}, \tag{1}$$

where $E_{\rm B}^{\rm i}$ is the binding energy of the adsorbate species $i$, usually expressed as a temperature ($T_{\rm B}^{\rm i} = E_{\rm B}^{\rm i}/k$), $T_{\rm dust}$ is the dust temperature and $\nu_0^{\rm i}$ is the vibration frequency of the adsorbed molecule given by

$$\nu_0^{\rm i} = \sqrt{2N_{\rm s}kT_{\rm B}^{\rm i}/\pi^2 m_{\rm i}}, \tag{2}$$

where $N_{\rm s}$ is the number of binding sites per unit area, and $m_{\rm i}$ is the mass of the adsorbed particle. Typically, $\nu_0 = 10^{12}$–$10^{13}$ s$^{-1}$.

Assuming that $T_{\rm dust} = T_{\rm peak} = 70$ K and $T_{\rm B} = 1200$ K for CO (as specified in HH93), with $N_{\rm s} = 10^{15}$ cm$^{-2}$ this yields $k_{\rm evap}^{\rm CO} \sim 3.1 \times 10^4$ s$^{-1}$, and the evaporation time-scale for one molecule ($1/k_{\rm evap}^{\rm CO}$) $\sim 3 \times 10^{-5}$ s. With these values of $T_{\rm dust}$ and $T_{\rm B}$, HH93 estimated that the cooling time-scale for a grain $t_{\rm cool} = 10^{-5}$ s$^{-1}$ (not to be confused with the evaporation time-scale per molecule). So with $t_{\rm impact} = 3.16 \times 10^{13}$ s (1 Myr), the duty cycle is $\sim 3.16 \times 10^{-19}$ and the value for the CO desorption rate as given in HH93 is obtained: $k_{\rm crd}^{\rm CO} = 9.8 \times 10^{-15}$ s$^{-1}$.

Finally, the volumetric evaporation rate (cm$^{-3}$ s$^{-1}$) of a species $i$ can be determined:

$$\dot{n}_{\rm i} = k_{\rm crd}^{\rm i}\sigma_{\rm H} n_{\rm H} N_{\rm s} f_{\rm i}, \tag{3}$$

where $f_{\rm i}$ is the fractional surface coverage of species $i$, $\sigma_{\rm H}$ is the grain surface area per hydrogen nucleon, and $n_{\rm H}$ is the hydrogen nucleon density. Or, expressed as the rate of change of the fractional abundance of the coolant species CO ($X_{\rm CO}$):

$$\dot{X}_{\rm CO} = k_{\rm crd}^{\rm CO}\sigma_{\rm H} N_{\rm s},$$

where we have assumed that $f_{\rm CO} = 1$.

Alternatively, the desorption rate can be determined by considering the energetics of the process. The advantage of such an approach is that (assuming the various assumptions listed above hold) the equivalent continuous desorption coefficient is simply defined by the number of CO molecules that are required to effect cooling ($N_{\rm CO}$), and the interval between cosmic ray impact/heating events – and is essentially independent of the details of the peak grain temperature and cooling time-scales etc. Thus, evaporation will continue until a sufficient number of CO molecules have been ejected so as to cool the grain.

Therefore:

$$N_{\rm CO}.kT_{\rm B}^{\rm CO} \sim f_{\rm E}.\Delta E,$$

where $f_{\rm E}$ is the fraction of the total deposited energy ($\Delta E$) that is removed by evaporative cooling in any one cooling cycle.

The cooling rate (whether by evaporative, or radiative cooling) is proportional to the grain surface area and the evaporation rate per molecule (e.g. equation 3 of Léger et al. 1985) so that, for a single grain:

$$\Gamma_{\rm CO} = \frac{{\rm d}E}{{\rm d}t} = k_{\rm evap}^{\rm CO}.4\pi a^2.N_{\rm s}.f_{\rm CO}.kT_{\rm B}^{\rm CO}, \tag{4}$$

where $a$ is the grain radius. The cooling time-scale ($t_{\rm cool}$) is then given by

$$t_{\rm cool} \sim \frac{f_{\rm E}.\Delta E}{\Gamma_{\rm CO}}.$$

Note that $t_{\rm cool}$ depends on *both* the evaporation rate and the grain surface area.

The number of molecules that are evaporated from a single grain in a period of time equal to $t_{\rm cool}$ is then given by

$$N_{\rm i} = k_{\rm evap}^{\rm i}.t_{\rm cool}.4\pi a^2.N_{\rm s} = k_{\rm crd}^{\rm i}.t_{\rm impact}.4\pi a^2.N_{\rm s}. \tag{5}$$

Identifying CO as the coolant species and using the values adopted by HH93; $T_{\rm B}^{\rm CO} = 1200$ K, $a = 0.1$ μm, $\Delta E = 0.4$ MeV, and $t_{\rm cool} = 10^{-5}$ s, a value of $f_{\rm E} = 0.1$ is implied. This gives $N_{\rm cool}^{\rm CO} \sim 3.9 \times 10^5$ and corresponds to cooling from a peak value of ~70.8 to ~67.1 K. These values of $f_{\rm E}$ and $N_{\rm cool}^{\rm CO}$ have probably been underestimated, as discussed in Section 4 below.

### 2.1.1 *Desorption rates for other species*

The same formalism described above can be used to determine the equivalent desorption rates for other species ($k_{\rm crd}^{\rm i}$) for a given grain

radius ($a$). The cooling and impact time-scales ($t_{\rm cool}$ and $t_{\rm impact}$) and hence the duty cycle are fixed, so that – given $k_{\rm crd}^{\rm CO}$ – the rates simply scale according to:

$$\frac{k_{\rm crd}^{\rm i}}{k_{\rm crd}^{\rm CO}} = \frac{k_{\rm evap}^{\rm i}}{k_{\rm evap}^{\rm CO}}$$

and

$$k_{\rm crd}^{\rm i} = k_{\rm crd}^{\rm CO}\left[\frac{T_{\rm B}^{\rm i}}{T_{\rm B}^{\rm CO}}\frac{m_{\rm CO}}{m_{\rm i}}\right]^{1/2}\exp\left(\frac{T_{\rm B}^{\rm CO}-T_{\rm B}^{\rm i}}{T_{\rm peak}}\right).$$

The values given in table 4 of HH93 can be retrieved using this simple relationship.

We should, however, note that even assuming the same values for the physical parameters as in HH93, there is considerable uncertainty in these rates and some other studies have yielded significantly different values. So, for example, by considering more localized ice mantle 'hotspot' heating Bringa & Johnson (2004) calculated a rate for $H_2O$ desorption that is approximately 30 times larger than the HH93 value. Alternatively, Herbst & Cuppen (2006) applied a detailed continuous-time random walk Monte Carlo approach to the heating of grains and the evaporation of molecules to obtain stochastic desorption rates. Using a different (and wider) spectrum of cosmic rays they determined larger cosmic ray fluxes (and hence a shorter $t_{\rm impact} = 10^5$ yr), and lower peak temperatures, but yielding a significantly larger value of $k_{\rm crd}^{\rm CO} = 5.7 \times 10^{-13}\,{\rm s}^{-1}$. In addition, there are considerable uncertainties in the rates deriving from assumptions about the grain morphology, size distribution, thermal connectivity, the nature and spectrum of the cosmic rays etc.

## 3 EXTENSION TO OTHER GRAIN SIZES

### 3.1 Dependence on the grain size

If we accept the 'late time, whole grain thermal desorption' physical model of HH93 and the various assumptions specified in the previous section hold, then it is fairly easy to adapt the formalism beyond the 'classical' scenario. The continuous desorption representation can thus be applied to different cosmic ray fluxes and grain sizes, so long as 25 K $\lesssim T_{\rm peak} \lesssim$ 150 K. This corresponds to impacts on grains with radii in the range 0.03 μm $\lesssim a \lesssim$ 0.25 μm.

However, the model cannot be extended to very small, or very large grains. There are several complicating issues for the small grains; first the 'granularity' of the stochastic nature of the process becomes more important; $t_{\rm impact}$ scales as the inverse of the geometric cross-section, so that for $a = 0.01$ μm, $t_{\rm impact} = 100$ Myr. This is very much larger than the time-scale for changes in the physical and chemical environment of the dust grains. Secondly, for grains smaller than $\sim 0.02$ μm, the radius of the cosmic ray 'impact cylinder' is comparable to the grain radius and the desorption efficiency may be much higher, due to the increased significance of the direct, impulsive desorption mechanisms (e.g. as described by Bringa & Johnson 2004). Thirdly, for the smallest grains, where $T_{\rm peak} \gtrsim$ 150–160 K, the situation is further complicated by the facts that desorption and cooling by the less volatile, but dominant bulk ice component, $H_2O$, may become important, depending on the assumptions concerning the binding energy and the nature of the desorption process. In addition, a greater proportion of the grain will be composed of ice, as opposed to refractory material, with a different cosmic ray stopping power. Fourthly, and perhaps most significantly, for the smallest grains there may be an insufficient number of molecules in the ice to allow efficient evaporative cooling. Together with the high peak temperatures and electron fluxes and the possibility of total grain disruption, these factors suggest that for these grains something akin to explosive whole mantle desorption may take place.

As small grains dominate the interstellar size distribution the implications are that the desorption of volatile species may be overestimated by the the HH93 formalism (due to the ice budget limitation), whilst that for strongly bound species – including complex organic molecules (COMs) – could be significantly underestimated (due to whole mantle desorption/grain disruption).

For the larger grains (where $T_{\rm peak} \lesssim 25$ K), radiative cooling starts to dominate over evaporative cooling, whilst for $a \gtrsim 0.25$ μm, 'cylinder/spot heating' and desorption at the cosmic ray entry/exit sites becomes more significant than whole grain heating. In addition, an additional term in the energy deposition should also be included due to the effects of lower energy cosmic rays, whose flux is ill-determined in dark cloud cores (Léger et al. 1985). Both these effects would result in significantly larger desorption rates than are predicted by the HH93 model.

However, within the range 0.03 μm $\lesssim a \lesssim$ 0.25 μm, and on the continued assumption that CO is the dominant ice component (and coolant) in the surface layers, we can easily scale the formulae discussed in the previous section to obtain the desorption rate for dust grains of different sizes.

As already noted, cosmic rays of a specific energy have an approximately uniform 'stopping power' or energy deposition rate per unit length (normalized to a deposition of $\Delta E = 0.4$ MeV, for a grain with $a = 0.1$ μm in HH93). Thus

$$\Delta E = 0.4\,{\rm MeV}\left(\frac{a}{0.1\,\mu{\rm m}}\right)\left(\frac{\zeta}{1.3\times10^{-17}\,{\rm s}^{-1}}\right). \quad (6)$$

The temperature-dependence of the specific heat of refractory dust grains is reasonably well-known (Léger et al. 1985) so that $T_{\rm peak}$ for grains of different sizes can easily be calculated for an appropriately scaled value of $\Delta E$ using the expression;

$$\Delta E = \frac{4}{3}\pi a^3\int_{T_0}^{T_{\rm peak}} C_{\rm vol.}\,T\,dT,$$

where $a$ is the grain radius, $C_{\rm vol.}$ is the volumetric heat capacity [in J cm$^{-3}$ K$^{-1}$, as given by equations 1a and b in Léger et al. (1985)], and $T_0$, $T_{\rm peak}$ are the initial and peak grain temperatures.

We then obtain (for $10 < T_{\rm peak} < 50$ K):

$$T_{\rm peak}^3 = 3.28\times10^5\left(\frac{a}{0.1\,\mu{\rm m}}\right)^{-2} + T_0^3 \quad (7)$$

and (for $50 < T_{\rm peak} < 150$ K):

$$T_{\rm peak}^{2.3} = 1.597\times10^4\left(\frac{a}{0.1\,\mu{\rm m}}\right)^{-2} + 4.87\times10^{-2}T_0^3 + 1990. \quad (8)$$

We also note, again assuming that CO is the dominant adsorbate and coolant species, that for an individual grain, $k_{\rm crd}^{\rm CO}$ and $N_{\rm cool}^{\rm CO}$ are simply related through equation (5). The interval between cosmic ray impacts is inversely proportional to the cross-sectional area of the grain, so that

$$t_{\rm impact} = 3.16\times10^{13}\left(\frac{0.1\,\mu{\rm m}}{a}\right)^2\left(\frac{1.3\times10^{-17}s^{-1}}{\zeta}\right). \quad (9)$$

Here it is important to note that the energy deposition ($\Delta E$), and hence $N_{\rm cool}^{\rm CO}$, are proportional to the grain radius ($a$), whilst the interval between cosmic ray impacts is inversely proportional to the grain cross-section ($t_{\rm impact} \propto a^{-2}$). Hence the CR-induced desorption rate coefficient $k_{\rm crd}^{\rm CO} \propto a$. The same dependency on grain radius can be deduced from equation (5) noting that the cooling time-scale ($t_{\rm cool}$)

for an individual grain depends on the energy deposition ($\propto a$) and the inverse of the grain surface area ($\propto a^{-2}$) as well as the evaporation time-scale (itself a function of the peak temperature and, hence, the grain radius).

This observation is different to what has been deduced/assumed in some recent studies (e.g. Zhao, Caselli & Li 2018; Sipilä, Zhao & Caselli 2020) which are based on the erroneous assumption that identifies the evaporation time-scale for the coolant molecule with the cooling time-scale for the grain, so that it does not have an explicit grain size-depenence. This was not claimed in HH93 and is self-evidently incorrect (the cooling time-scale being proportional to the evaporation time-scale divided by the grain radius, as described above) – e.g. see equation (3) of Léger et al. (1985). The source of this confusion is almost certainly due to the fact that, for 0.1 μm grains, and with the parameters used in HH93, *both* time-scales are of the order of $10^{-5}$ s$^{-1}$. Obviously, this error is unimportant in the context of models that duplicate the parameters used in HH93, but it has serious implications when scaling the results for different species, grains sizes and cosmic ray spectra etc. Consequently, compared to previous studies, we obtain somewhat different results for the desorption rates averaged over representative grain size population distributions.

### 3.2 Application to grain size distributions

In molecular clouds where the effects of ice grain coagulation/agglomeration are not significant, an empirically constrained fit to the observed interstellar extinction curve is given by a simple power-law distribution of (uncoated) dust grain sizes (Mathis, Rumpl & Nordsieck 1977), hereafter MRN, so that the number of grains with radii between $a$ and $a + da$ is given by $n(a)\mathrm{d}a = n_0 a^{-3.5}$ defined within the approximate limits of $0.005\ \mu\mathrm{m} < a < 1.0\ \mu\mathrm{m}$.

Ideally, the gas–grain interactions – including the accumulation and composition of ices should be followed for a population of dust grains of different sizes, weighted according to the grain size distribution. Unfortunately, the microscopic description of freeze-out and desorption of a multigrain fluid becomes extremely complicated once the sporadic nature of the process is taken into account, and all the more so in dynamically evolving environments where the dynamical time-scales may be comparable, or less than, the time-scale between cosmic ray heating events ($t_{\mathrm{impact}}$).

However, in the simplified case of assumed continuous desorption from homogeneous ice mantles we can obtain order-of-magnitude estimates for the population-averaged desorption rates. For the MRN distribution, and depending on the limits of the distribution, the value of the implied dust surface area per hydrogen nucleon ($\sigma_{\mathrm{H}}$) lies in the range $3\text{–}8 \times 10^{-21}$ cm$^2$. We adopt a standard value of $6.0 \times 10^{-21}$ cm$^2$ in this study.

We can compare the value of the cosmic ray desorption rate for CO averaged over this distribution ($k_{\mathrm{crd}}^{\mathrm{CO}}$), to that obtained for a single size grain distribution ($a = 0.1$ μm, as used by HH93) on the assumption that both distributions yield (i) the same value of the dust-to-gas ratio (by mass), or (ii) the same surface area per hydrogen nucleon.

Using the assumption of a fixed dust-to-gas mass ratio we note that, since the product of $k_{\mathrm{crd}}^{\mathrm{CO}}.4\pi a^2$ scales as $a^3$, as does the dust mass distribution, then, $\overline{k_{\mathrm{crd}}^{\mathrm{CO}}} = k_{\mathrm{crd}}^{\mathrm{CO}}(0.1\ \mu\mathrm{m})$, irrespective of the grain size distribution.

Alternatively, assuming that the grain surface area is fixed, then we obtain:

$$\overline{k_{\mathrm{crd}}^{\mathrm{CO}}} = \frac{\int k_{\mathrm{crd}}^{\mathrm{CO}}(a).4\pi a^2.n(a)\mathrm{d}a}{\int 4\pi a^2.n(a)\mathrm{d}a} \qquad (10)$$

so that, with $k_{\mathrm{crd}}^{\mathrm{CO}}(a) \propto a$, this gives:

$$\overline{k_{\mathrm{crd}}^{\mathrm{CO}}} = k_{\mathrm{crd}}^{\mathrm{CO}}(0.1\ \mu\mathrm{m})\frac{\sqrt{a_{\mathrm{min}}a_{\mathrm{max}}}}{a_0}.$$

Using a slightly truncated MRN distribution (for the reasons described above), with $a_{\mathrm{min}} = 0.03$ μm and $a_{\mathrm{max}} = 0.25$ μm we obtain $\overline{k_{\mathrm{crd}}^{\mathrm{CO}}} = 0.87k_{\mathrm{crd}}^{\mathrm{CO}}(0.1\ \mu\mathrm{m})$. Note, however, that the ratio is close to unity and is fairly insensitive to the assumed range of the grain size distribution. e.g. for $0.02\ \mu\mathrm{m} < a < 0.25\ \mu\mathrm{m}$: $\overline{k_{\mathrm{crd}}^{\mathrm{CO}}} = 0.71k_{\mathrm{crd}}^{\mathrm{CO}}(0.1\ \mu\mathrm{m})$, whilst for $0.03\ \mu\mathrm{m} < a < 0.5\ \mu\mathrm{m}$: $\overline{k_{\mathrm{crd}}^{\mathrm{CO}}} = 1.22k_{\mathrm{crd}}^{\mathrm{CO}}(0.1\ \mu\mathrm{m})$.

Previous studies, based on the different understanding of the cooling time-scale (e.g. Zhao et al. 2018), have obtained slightly different results for the population-averaged rate for the principle desorbate and coolant; CO. Thus $\overline{k_{\mathrm{crd}}^{\mathrm{CO}}} = 1.05k_{\mathrm{crd}}^{\mathrm{CO}}(0.1\ \mu\mathrm{m})$. Although, in the case of CO, this discrepancy is small there is a very significant qualitative difference between the two approaches; as pointed out above, studies which do not include an explicit grain size-dependence of $t_{\mathrm{cool}}$ yield $k_{\mathrm{crd}}^{\mathrm{CO}} \propto a^2$. Thus, for an MRN-type of grain size distribution, the integrand in the numerator of equation (10) is $\propto a^{0.5}$ and the desorption is therefore weighted towards the larger grains in the distribution (Sipilä et al. 2020). However, we find that $k_{\mathrm{crd}}^{\mathrm{CO}} \propto a$ and the integrand is $\propto a^{-0.5}$ so that it is the *smaller* grains that contribute most to the population-averaged desorption rates.

This is an important point since, as we have already noted, the physics of the desorption process become complex and are ill-defined for the smallest grains. Additional complications will arise from the fact that, compared to the larger grains, it is likely that the composition of the surface layers of the ices will be quite different for the smallest grains. The significance of the smaller grains will be slightly slightly reduced due to the fact that for these grains the ice, which has a lower cosmic ray 'stopping power' than refractory material, makes up a greater proportion of the total (ice + refractory) volume of the mantled grains. This mitigation will not, however, diminish the fundamental conclusion that small grains dominate the desorption. Moreover, it should also be noted that cosmic rays of different energies (and with lower stopping powers) will be more able to heat small grains to temperatures sufficient for evaporation to occur, further biasing the desorption towards the small grain population.

As stated above, the differences are not particularly strong in the case of CO, but the situation is obviously much more complicated for other (less abundant) species in the ices. For these species, the desorption and cooling are not closely coupled as they are in the case of CO. In general, they will have different binding energies and hence different dependencies of the sublimation rate on the peak dust temperature that (unlike CO) are not so strongly constrained by the balance between deposition energy and number of molecules that are desorbed. As the smaller grains (with higher peak temperatures) dominate, this implies that population-averaged desorption rates for species with $E_{\mathrm{B}}^{\mathrm{i}} > E_{\mathrm{B}}^{\mathrm{CO}}$ have probably been strongly underestimated in previous studies, and we investigate this possibility in the next section.

## 4 REVISION OF THE CONTINUOUS DESORPTION MODEL

The representation of cosmic ray induced desorption, which is an intermittent, stochastic, process by a continuous desorption formulation was implemented for the sake of simplicity and ease of use in astrochemical models of time-dependent chemistry where

rate equation descriptions are employed. We have already noted that several assumptions and simplifications have been made, notably that the desorption is primarily driven by whole grain heating. The inclusion of other desorption mechanisms (e.g. as described by Bringa & Johnson 2004) implies that there is potentially a very wide range in the theoretically determined value of $k_{\rm crd}^{\rm CO}$.

However, even within the context of the HH93 model, there are some limitations and unqualified assumptions which we identify and discuss in this section. The issues that we address are:

(i) consideration of limitations to the desorption rates set by the availability of the desorbed species and/or coolant molecules,
(ii) underestimation of the cooling time-scale (and hence the period of time during which mantle desorption occurs),
(iii) the treatment of sporadic desorption as a continuous process,
(iv) the possibility of species co-desorption, and
(v) special consideration of very small grains.

We consider all of these points in this study. In addition, it should also be noted that the HH93 model was limited to consideration of grains of one size, being impacted by cosmic rays of a single type and energy. This limitation has been addressed in recent studies (e.g. Silsbee, Caselli & Ivlev 2021) but here we note that, in addition to the additional uncertainties concerning the characeristics and attenuation of the cosmic ray energy spectrum, the dust grain size population, and their thermal properties etc., the large uncertainties inherent in the above list may limit the value of such studies. Therefore, for the purpose of this study, we have not included a discussion of these issues.

### 4.1 Compositional limitations

Due to the stochastic nature of the cosmic ray induced desorption process, the desorption rate for any species dictated at the microscopic level and is necessarily limited by the energy budget and the availability of that species. Clearly, the continuous desorption model becomes meaningless if it effectively translates to a situation in which the implied number of desorptions per cosmic ray impact/event exceeds the number of molecules in the ice mantle.

As previously noted; for the range of desorption temperatures that we consider, evaporative cooling is the dominant cooling mechanism (Léger et al. 1985). Thus, for a single grain, the product of $k_{\rm evap}^{\rm cool}.t_{\rm cool}$ is determined by the requirement that the number of desorbed molecules multiplied by their binding energy is some fraction of the energy deposition ($\Delta E$). For $\Delta E \sim 0.4$ MeV, this equates to $\sim 10^6$ CO molecules in the HH93 model (assuming that CO is the dominant volatile component of the ice, and therefore the dominant coolant). This is a large number; the formalism therefore only holds if there are $\gtrsim 10^6$ CO molecules in the ice before the desorption event starts. This is a non-trivial requirement. Continuing with the assumption that CO is the dominant evaporate and coolant, we can compare $N_{\rm cool}^{\rm CO}$ with the number of available binding sites in the surface layers of the ice. Assuming that the total ice thickness is significantly less than the bare grain radius ($a_0$), which is true for classical 0.1-μm grains, then:

$$N_{\rm cool}^{\rm CO} = 4\pi a^2 . N_{\rm s} . f_{\rm CO} . n_{\rm L}$$

where $n_{\rm L}$ is the number of ice layers, and $f_{\rm CO}$ is the fractional surface coverage of CO. With the values given in Table 1 and assuming a pure CO ice ($f_{\rm CO} = 1$) then

$$N_{\rm cool}^{\rm CO} = 1.26 \times 10^6 n_{\rm L}.$$

**Table 1.** Parameters for the models.

| Parameter | Value |
|---|---|
| Helium abundance (He/H) | 0.1 |
| Carbon abundance (C/H) | $1.5 \times 10^{-4}$ |
| Nitrogen abundance (N/H) | $7.4 \times 10^{-5}$ |
| Oxygen abundance (O/H) | $2.5 \times 10^{-4}$ |
| Sulfur abundance (S/H) | $1.0 \times 10^{-7}$ |
| Sodium abundance (Na/H) | $1.0 \times 10^{-8}$ |
| Gas temperature ($T_{\rm g}$) | 10 K |
| Initial dust temperature ($T_{\rm d}^0$) | 10 K |
| Minimum temperature for evap. cooling ($T_{\rm d}^{\rm min}$) | 25 K |
| Cosmic ray ionization rate ($\zeta$) | $1.3 \times 10^{-17}$ s$^{-1}$ |
| Dust surface area per hydrogen nucleon ($\sigma_{\rm H}$) | $6.0 \times 10^{-21}$ cm$^{-2}$ |
| Surface density of binding sites ($N_{\rm s}$) | $10^{15}$ cm$^{-2}$ |
| Ice layer thickness ($\Delta a$) | 3.7 Å |
| Mean dust grain albedo ($\omega$) | 0.5 |

Thus, each desorption event would result in the sublimation of ∼1 monolayer of ice. Indeed if, as discussed below, $t_{\rm cool}$ is significantly larger than the values used in HH93, this required level of desorption may amount to several layers of ice (in the case of classical grains) or even exceed the available ice reservoir (in the case of the smallest grains). Throughout this discussion we must remember that the model is only appropriate to those regions where there are substantial depositions of ices in which CO is the dominant component. This is likely to be true in the darkest, coldest, and most dense parts of molecular clouds/quiescent star-forming regions.

The situation becomes even more complicated for low abundance volatile species which, to satisfy the implied desorption rate, may need to be 'excavated' from sub-surface levels, raising the issue of the diffusion of species from the mantle interiors to the surfaces. The importance of the 'budgetary limitation' can most clearly be seen if we consider the desorption of highly volatile species. For example, atomic hydrogen, which has a very low surface binding energy, will have – according to the HH93 formulation – a very high value of $k_{\rm crd}^{\rm H} \sim 6.0 \times 10^{-9}$ s$^{-1}$. This would effectively mean that, in the continuous desorption representation, H atoms would be absent from ices. So, in table 5 of HH93 we see that, by balancing the desorption and accretion rates, the ratio of gaseous to surface abundances of H atoms would be $1.6 \times 10^4$. Since the gas-phase abundance of H atoms in dark clouds is typically ∼1 cm$^{-3}$, this implies a surface abundance of H-atoms that is so low as to preclude the existence of surface hydrogenation reactions. In reality, so long as the time-scale for accretion is less than the cosmic ray impact time-scale, H atoms would accrete on to cold grains and build up a substantial surface abundance for most of the desorption cycle, only being (efficiently) sublimated at each desorption event.

We can calculate the *maximum possible* value for $k_{\rm crd}^{\rm i}$, based on the extreme, yet unlikely, situation of *complete* mantle desorption. Here we consider the corresponding equivalent desorption rates and then simply state that the continuous desoprtion rates that we have calculated above cannot possibly exceed these values. In that case, the injection of species $i$ (cm$^{-3}$, per desorption event) is

$$\Delta n_{\rm i} = (X_{\rm ice}^{\rm i})_0 . n_{\rm H},$$

where $(X_{\rm ice}^{\rm i})_0$ is the fractional abundance of species $i$ in the solid state, at the time of the desorption event (and, obviously, assuming that there is no continuous cosmic ray induced desorption). Thus, with the assumption that $n_{\rm H}$ is not time-dependent, this equates to

$$\dot{n}_{\rm i} = \frac{(X_{\rm ice}^{\rm i})_0 . n_{\rm H}}{t_{\rm impact}}.$$

Comparing this to the continuous cosmic ray induced desorption rate, given by equation (3), we obtain

$$k^{\rm i}_{\rm crd}({\rm max}) = \frac{(X^{\rm i}_{\rm ice})_0}{\sigma_{\rm H} N_{\rm s} t_{\rm impact} f_{\rm i}}.$$

Adopting values from Table 1 and making the assumptions that (a) the ice is well-mixed so that $f_{\rm i}$ is approximately equal to $(X^{\rm i}_{\rm ice})_0$ divided by the total ice abundance, and (b) most of the oxygen has frozen out (predominantly in the forms of $H_2O$ or CO), so that the total ice abundance is $\sim 2 \times 10^{-4}$, then we find

$$k^{\rm i}_{\rm crd}({\rm max}) \sim 1.0 \times 10^{-12} \left(\frac{a}{0.1\,\mu{\rm m}}\right)^2 \left(\frac{\zeta}{1.3 \times 10^{-17} s^{-1}}\right) = \left(\frac{33.3}{t_{\rm impact}}\right). \quad (11)$$

It is important to realize that this is an extreme upper limit and so is quite a stringent constraint. It therefore implies that the values given in HH93 for the desorption rates for highly volatile species such as H, $H_2$, He, C, N, O, CH, NH, and $NH_2$ are greatly overestimated. Indeed, if one adopts the larger value of $t_{\rm cool}$ discussed above and considers the smaller grains ($a \sim 0.03\,\mu$m) then this upper limit will be important for dominant ice components such as $CH_4$, $N_2$, $NH_3$, and even CO. Moreover, we should also be aware that the volatile ice components are probably more abundant in the outer layers of the ice than they are in the interior, further reducing the implied value of $k^{\rm i}_{\rm crd}({\rm max})$.

### 4.2 Extended cooling

In the HH93 study the cooling time-scale ($t_{\rm cool}$) was very loosely defined and both it and the number of coolant molecules sublimated from the surface ($N_{\rm cool}$) have probably been significantly underestimated. The value of $t_{\rm cool} \sim 10^{-5}$ s used in HH93 corresponds to a drop in temperature of a grain of radius $a = 0.1\,\mu$m from its peak value of ~70 to ~67.1K, a reduction of the evaporation rate by a factor of ~2, and ~10 per cent of the energy deposited by a cosmic ray impact being lost through evaporative cooling (i.e. $f_{\rm E} \sim 0.1$). Indeed, by the time that the dust grain temperature has fallen to 60 K, some $\sim 1.3 \times 10^6$ molecules will have evaporated and the evaporation rate will have fallen to ~6 per cent of its peak value.

However, even at this level, the implied cooling time-scale is still many orders of magnitude less than the time-scales for either freeze-out, or cosmic ray impacts ($t_{\rm impact}$) so that evaporation will continue until radiative cooling starts to become significant and/or the rate of freeze-out of the coolant species becomes comparable to the evaporation rate. For the classical (0.1 μm) grains that were the basis of the Léger et al. (1985) study radiative cooling only becomes dominant once the grain temperature has fallen to ~25 K. More detailed recent studies (e.g. Kalvāns & Kalnin 2020b; Sipilä, Silsbee & Caselli 2021) suggest that the threshold temperature may be somewhat higher although, as discussed below, the desorption rates are very insensitive to this value. The rate of freeze-out (${\rm cm^{-3}\,s^{-1}}$) of a neutral species, $i$, is given by

$$\dot{n}_{\rm i} = -n_{\rm H} n_{\rm i} \sigma_{\rm H} S_{\rm i} \left(\frac{k T_{\rm g}}{2\pi m_{\rm i}}\right)^{1/2},$$

where $S_{\rm i}$ is the sticking coefficient (typically assumed to be ~1), and $T_{\rm g}$ is the gas kinetic temperature. With the values of $\sigma_{\rm H}$ and $T_{\rm g}$ given in Table 1 the freeze-out time-scale for CO (when $d(n_{\rm CO}) \sim n_{\rm CO}$) is thus

$$\tau^{\rm CO}_{\rm fo} = 2.4 \times 10^4 \left(\frac{10^5 {\rm cm^{-3}}}{n_{\rm H}}\right) {\rm yr}.$$

With our assumption that the coolant species is CO with a binding energy of $T_{\rm B} = 1100$ K, the gas temperature is 10 K, the sticking coefficient $S_{\rm CO} = 1$, the ice is composed of CO only and that there has been efficient conversion of C to CO in the gas phase, then the freeze-out and desorption rates are equal when $T_{\rm dust} \sim$ 20–22 over the gas density range $n_{\rm H} = 10^5$–$10^7$ ${\rm cm^{-3}}$.

We therefore adopt a value of $T^{\rm min}_{\rm D} = 25$ K in this study. Cooling from the peak temperature of ~70 K to this value then corresponds to $f_{\rm E} \sim 0.95$ – that is to say, evaporative cooling can effectively remove nearly all of the deposited impact energy. In fact, as shown below, the total time-integrated desorption rate is not at all sensitive to the value of $T^{\rm min}_{\rm D}$ as the great majority of the evaporation occurs the higher temperatures, due to the exponential form of the evaporation rate. In any case, this is significantly larger than the value of $f_{\rm E} \sim 0.1$ adopted in HH93 which implies that the desorption rates may be of the of the order of ~10 × larger than those determined in that study.

To quantify the total desorption rate, integrated through an impact/cooling cycle, rather than assume that the desorption of all species occurs at a fixed temperature ($T_{\rm peak}$) for a single time period ($t_{\rm cool}$), we have performed calculations that determine the time-dependence of the dust grain temperature ($T_{\rm d}$) and hence the number of molecules desorbed as a function of time for each species, integrated from $T_{\rm peak}$ to $T^{\rm min}_{\rm d}$. This approach is applicable, so long as the cooling time-scale is significantly less than those for the gas-phase chemistry and freeze-out, or the interval between cosmic ray impacts. The total number of molecules desorbed from a grain per heating event can then be converted to an effective continuous desorption rate using the above formulae.

The relationships between the grain temperature and energy (in J) can be derived from equations (6), (7), and (8): For $T_{\rm d} \leq 50$ K

$$T_{\rm d} = 1.724 \times 10^6 \left(\frac{0.1\,\mu{\rm m}}{a}\right) E^{1/3} \quad (12)$$

whilst for $50 < T_{\rm d} \leq 150$ K,

$$T_{\rm d} = \left[2.5 \times 10^{17} E \left(\frac{0.1\,\mu{\rm m}}{a}\right)^3 + 1990.25\right]^{1/2.3}. \quad (13)$$

The initial increment in the thermal energy and the peak dust temperature are defined by the energy deposition per cosmic ray impact ($\Delta E$). The initial (pre-impact) temperature of dust grains is taken to be $T^0_{\rm d} = 10$ K. For our purposes we assume that the cooling rate (and hence the desorption rates) are determined on the basis of pure evaporative cooling by a single coolant species (typically CO) with an invariant binding energy, that dominates the composition of the surface layers of the ice mantles. As shown below, this is a reasonably fair approximation.

With this assumption, the evaporation rate ($s^{-1}$) for the coolant species is given by equation (1). The desorption rate for a single grain is then given by

$$\dot{n}_{\rm cool} \sim k^{\rm cool}_{\rm evap}.4\pi a^2 N_{\rm s}$$

and the cooling rate is given by equation (4) (with $f_{\rm CO} = 1$). Thus, the time-dependence of the dust temperature and the total cumulative desorption of the coolant species (and other species, using the same formalism) can easily be determined.

Table 2 shows how the dust grain temperature and number of coolant molecules that are evaporated ($N_{\rm cool}$) varies with time following the impact of a cosmic ray for two values of the coolant molecule binding energy: (a) 1100 K, and (b) 1200 K. These calculations have been performed assuming 'classical' (0.1 μm) dust grains and track the the cooling and desorption of the various species from $T_{\rm d} = T_{\rm peak} = 70.6$ K, down to $T_{\rm d} = T^{\rm min}_{\rm d} = 25$ K.

**Table 2.** The time-dependence of the dust temperature and the number of desorbed coolant molecules per grain, for a grain radius of $a = 0.1$ μm.

| $T_B^{cool} = 1100$ K | | | $T_B^{cool} = 1200$ K | | |
|---|---|---|---|---|---|
| Time (s) | $T_{dust}$ (K) | $N_{cool}$ | Time (s) | $T_{dust}$ (K) | $N_{cool}$ |
| 2.3(−7) | 70.6 | 4.2(4) | 9.6(−7) | 70.6 | 3.8(4) |
| 1.3(−6) | 69.6 | 2.1(5) | 5.4(−6) | 69.6 | 1.9(5) |
| 3.0(−6) | 68.2 | 4.0(5) | 1.3(−5) | 68.2 | 3.7(5) |
| 7.9(−6) | 65.7 | 7.7(5) | 3.5(−5) | 65.7 | 7.0(5) |
| 5.7(−5) | 58.8 | 1.7(6) | 2.9(−4) | 58.8 | 1.5(6) |
| 1.1(−3) | 49.5 | 2.7(6) | 8.1(−3) | 49.5 | 2.4(6) |
| 1.9(5) | 25.0 | 4.0(6) | 1.2(7) | 25.0 | 3.7(6) |

As can be seen from this table, the full cooling time-scale (to reach $T_d^{min}$) is quite long ($\sim 10^5$–$10^7$ s) and moderately sensitive to the value of $T_B^{cool}$ (particularly once $T_d \lesssim 50$ K), although it is many orders of magnitude smaller than the time-scale for gas-phase chemical processes, or for the freeze-out of molecules on to grains, ($\tau_{fo}^{CO}$) or the interval between cosmic ray heating events ($t_{impact}$). In any case it is important to note that, in both cases, the great majority of the coolant molecules are evaporated within a few milliseconds. This implies that the assumed value of $T_d^{min}$ is not critical to the determination of the desorption rates. The table also confirms our observation that the total level of desorption (and hence cooling) at the nominal value of $t_{cool} = 10^{-5}$ s adopted by HH93, is approximately a factor of 10× less than the value obtained when the full cooling to $T_d^{min}$ is considered.

These calculations were repeated for grains with different radii within the specified range ($0.03 < a < 0.25$ μm), with appropriate scaling for the energy deposition (as given by equation 6), and the interval between cosmic ray impacts (as given by equation 9). The total number of of each species that is desorbed per impact/heating event ($N_i$) can then be converted to an equivalent continuous desorption rate using equation (5). The values calculated in this way were limited so as to be less than the maximum value of $k_{crd}^{i}$(max) given by equation (11) above. Results from these calculations are shown in Tables 3, 4, and 5. These give the equivalent desorption rates calculated using the full cooling calculation for the lower and upper limits of the assumed grain size distribution (0.03 and 0.25 μm) as well as for the nominal 'classical' grain size of 0.1 μm.

Table 3 shows the results obtained for selected species. For these calculations, and in most of the models described below, we have used the binding energies given in HH93. Whilst we recognize that some of these values have been updated in recent years we have taken this approach for ease of comparison and to identify the significance of the effects of extended cooling and/or the capping of the desorption rates described above. However, in the case of $H_2O$, the value used in HH93 ($T_B^{H_2O} = 1860$ K) is significantly lower (albeit possibly applicable to mixed ices) than the values currently adopted. We therefore use $T_B^{H_2O} = 4800$ K (Minissale et al. 2016), but also include results obtained using the HH93 value, designated $H_2O^{\dagger}$, for comparison. The table includes, again for comparison, the desorption rates given in table 4 of HH93. These were calculated for a grain size of 0.1 μm and so should be compared to the extended cooling calculations for $a = 0.1$ μm. Note that some of the values in this table and also Tables 4 and 5 have been 'capped' at the maximum value, as given by equation (11).

As expected, the extended cooling results in an increase in the rates for volatile species (such as CO, $N_2$, and $NH_3$) by approximately an order of magnitude, whereas the rates for more tightly bound species (such as $H_2O$, $H_2S$, and $CO_2$) are only larger by a factor of $\lesssim 2\times$. For these species, the desorption rates fall very rapidly soon after the grain temperature drops from its peak value and little desorption occurs in the extended cooling period. For the same reason, the desorption rates for these species are much more strongly sensitive to the grain size than they are for the volatile species: the smaller grains have higher peak temperatures so that desorption of tightly bound species can persist for a longer fraction of the cooling period.

In these tables we also include the value for the desorption rates averaged over an MRN grain size distribution, as given by equation (10). It should be noted, however, that these values are highly uncertain due to (a) the assumed limits of the grain size distribution: we adopt $0.03\mu m < a < 0.25$ μm, for the reasons given above, but if – for example – the lower limit is reduced to 0.01 μm, then the mean rates would be reduced by a factor of ∼2 for weakly bound species (such as CO and $N_2$) but enhanced by an order of magnitude or more for strongly bound species (such as $H_2O$ and HCS) as one approaches the total desorption limit for the smallest grains, and (b) the assumption that the composition of the surface layers of the ice is independent of the the grain size. In fact, in the case of the simple model that we investigate below, this approximation is reasonably accurate.

Looking at the table, we can see that the MRN-weighted desorption rates are similar to the rates for 0.1- μm grains for the volatile species but are very much larger (in some cases by several orders of magnitude) for the more tightly bound species. As explained above, the rates for these species are much larger for the smaller grains in the distribution – and the average over the distribution places more weight on these small grains.

As a general result, it should be noted that the combined effects of including an extended cooling profile and averaging over a grain size distribution are to result in significantly larger values of the desorption rates for both volatile species (primarily due to the extended cooling) and tightly bound species (due to the contributions from small grains) and to yield a narrower range of rates than found in previous studies.

Unfortunately, there is is considerable uncertainty in the binding energies for the various species, and especially in mixed composition (predominantly apolar) ices. Therefore, in Table 4 we give the calculated desorption rates as a function of binding energy for a species of mass 10 amu, and assuming that the mean coolant species binding energy is 1200 K. Whilst the rates depend on both the binding energy ($T_B$) and the mass ($m_i$), the mass-dependence is only present in the vibration frequency of the adsorbed molecule ($\nu_0 \propto m_i^{-1/2}$; equation 2). This may therefore be more useful for astrochemical modelling purposes; for a specified binding energy, a value of the desorption rate (either for 'classical', 0.1- μm grains, or MRN-averaged) can be taken from this table and then scaled according to

$$k_{crd}^{i} = \left(\frac{10 \text{ amu}}{m_i}\right)^{1/2} k_{crd}^{10amu}$$

(subject to $k_{crd}^{i} \leq k_{crd}^{max}$) where $m_i$ is the mass of the species (in amu).

The binding energy of the coolant species (assumed to be CO) is, itself, quite uncertain – especially in mixed ices – and so results obtained for a binding energy of 1100 K are shown in Table 5 for comparison. This shows that for species with $T_B \lesssim 1200$ K, the rates are ∼5–10× smaller, although for species with larger binding energies the difference is $\lesssim 2\times$.

### 4.3 Sporadic desorption and ice species co-desorption

There is obviously a discrepancy between the sporadic, instantaneous, sublimation of the surface layer(s) of ices and its representation by a continuous surface desorption operating over the entire cycle, during which the physical conditions and composition of the

**Table 3.** Cosmic ray desorption rates ($s^{-1}$) for selected species with extended cooling times. $T_{bind}$ is the adopted binding energy (in K) for the species (taken from HH93 – but see text in section 4.2 for $H_2O$). Values are given for grain sizes of 0.01, 0.1, 0.25 μm and averaged over an MRN size distribution. Those labelled with a ⋆ are upper limits. Rates from HH93 are also given, for comparison.

| Species | $T_{bind}$ (K) | k (HH93) | k (0.03 μm) | k (0.1 μm) | k (0.25 μm) | k (MRN) |
|---|---|---|---|---|---|---|
| CO | 1210 | 9.8(−15) | 2.9(−14) | 9.2(−14) | 1.7(−13) | 7.3(−14) |
| $CH_4$ | 1360 | 1.6(−15) | 1.3(−14) | 8.5(−15) | 2.4(−15) | 1.0(−14) |
| $NH_3$ | 1110 | 5.0(−14) | 9.0(−14)⋆ | 9.9(−13) | 5.3(−12) | 9.3(−13) |
| $N_2$ | 1210 | 9.8(−15) | 2.9(−14) | 9.2(−14) | 1.7(−13) | 7.3(−14) |
| SiO | 3500 | 8.2(−29) | 4.3(−20) | 9.0(−29) | 4.4(−41) | 8.9(−21) |
| $H_2CO$ | 1760 | 4.4(−18) | 8.0(−16) | 1.2(−17) | 1.9(−20) | 2.6(−16) |
| $CO_2$ | 2500 | 1.1(−22) | 1.0(−17) | 1.7(−22) | 2.5(−29) | 2.3(−18) |
| HCN | 1760 | 4.6(−18) | 8.4(−16) | 1.2(−17) | 2.1(−20) | 2.8(−16) |
| HNC | 1510 | 1.5(−16) | 3.8(−15) | 5.8(−16) | 2.4(−17) | 1.8(−15) |
| HNO | 1510 | 1.4(−16) | 3.6(−15) | 5.4(−16) | 2.2(−17) | 1.7(−15) |
| $H_2S$ | 1800 | 2.4(−18) | 5.9(−16) | 5.9(−18) | 6.0(−21) | 1.9(−16) |
| $C_2S$ | 2500 | 9.8(−23) | 8.8(−18) | 1.5(−22) | 2.2(−29) | 2.0(−18) |
| HCS | 2000 | 1.2(−19) | 1.6(−16) | 2.6(−19) | 2.1(−23) | 4.5(−17) |
| O | 800 | 3.7(−12) | 9.0(−14)⋆ | 1.0(−12)⋆ | 6.3(−12)⋆ | 9.8(−13)⋆ |
| OH | 1260 | 6.3(−15) | 2.5(−14) | 4.7(−14) | 4.7(−14) | 3.8(−14) |
| $O_2$ | 1210 | 9.1(−15) | 2.7(−14) | 8.6(−14) | 1.6(−13) | 6.8(−14) |
| $H_2O^{\dagger}$ | 1860 | 1.4(−18) | 5.8(−16) | 3.3(−18) | 1.6(−21) | 1.7(−16) |
| $H_2O$ | 4800 | – | 6.4(−23) | 1.2(−36) | 4.6(−56) | 1.3(−23) |

**Table 4.** Cosmic ray desorption rates ($s^{-1}$) for a species of mass 10 amu as a function of binding energy for extended cooling times, with $T_B^{cool} = 1200$ K. Values are given for grain sizes of 0.01, 0.1, and 0.25 μm and averaged over an MRN size distribution. Those labelled with a ⋆ are upper limits.

| $T_{bind}$ (K) | k (0.03 μm) | k (0.1 μm) | k (0.25 μm) | k (MRN) |
|---|---|---|---|---|
| ≤1100 | 9.0(−14)⋆ | 1.0(−12)⋆ | 6.3(−12)⋆ | 9.8(−13)⋆ |
| 1200 | 4.9(−14) | 1.6(−13) | 2.9(−13) | 1.2(−13) |
| 1400 | 1.2(−14) | 4.7(−15) | 7.0(−16) | 7.5(−15) |
| 1600 | 3.4(−15) | 2.0(−16) | 2.3(−18) | 1.3(−15) |
| 1800 | 1.0(−15) | 9.5(−18) | 8.5(−21) | 3.3(−16) |
| 2000 | 3.3(−16) | 4.8(−19) | 3.4(−23) | 9.0(−17) |
| 2200 | 1.1(−16) | 2.5(−20) | 1.4(−25) | 2.7(−17) |
| 2400 | 3.5(−17) | 1.3(−21) | 6.0(−28) | 8.2(−18) |
| 2600 | 1.2(−17) | 7.2(−23) | 2.6(−30) | 2.6(−18) |
| 2800 | 3.8(−18) | 4.0(−24) | 1.2(−32) | 8.5(−19) |
| 3000 | 1.3(−18) | 2.2(−25) | 5.2(−35) | 2.8(−19) |
| 3500 | 8.6(−20) | 1.7(−28) | 7.2(−41) | 1.8(−20) |

**Table 5.** Cosmic ray desorption rates ($s^{-1}$) for a species of mass 10 amu as a function of binding energy for extended cooling times, with $T_B^{cool} = 1100$ K. Values are given for grain sizes of 0.01, 0.1, 0.25 μm and averaged over an MRN size distribution. Those labelled with a ⋆ are upper limits.

| $T_{bind}$ (K) | k (0.03 μm) | k (0.1 μm) | k (0.25 μm) | k (MRN) |
|---|---|---|---|---|
| ≤ 1000 | 9.0(−14)⋆ | 1.0(−12)⋆ | 6.3(−12)⋆ | 9.8(−13)⋆ |
| 1100 | 5.3(−14) | 1.7(−13) | 3.1(−13) | 1.3(−13) |
| 1200 | 2.5(−14) | 2.8(−14) | 1.5(−14) | 2.6(−14) |
| 1400 | 6.9(−15) | 1.1(−15) | 4.3(−17) | 3.3(−15) |
| 1600 | 2.1(−15) | 4.8(−17) | 1.5(−19) | 7.2(−16) |

surface layers of the ice mantles are liable to change. Notably, if the chemical time-scales and in particular, that for freeze-out, are comparable or longer than the cosmic ray impact time-scale then we can envisage that the effects of successive desorption events may be able to accumulate.

Moreover, the notion that the thermal desorption rate of each species is defined by the single composition binding energy of that species is simplistic and unsupported by laboratory data. These show that the desorption properties of different species are coupled so that, in many cases, they tend to sublimate in several, distinct, 'co-desorption bands' (Collings 2004; Viti et al. 2004; Öberg et al. 2005; Collings et al. 2015). Indeed, the various binding energies that are reported are highly uncertain and are usually defined for pure ice compositions and/or binding to bare refractory grain surfaces. In the first-order evaporative desorption mechanism, the vibration/binding characteristics are defined in the context of the molecular environment. Thus, the binding energies are not intrinsic but, instead, depend upon the composition of, and the degree of segregation within, the ices. If, for example, we consider a situation in which a polar molecule with a large binding energy (such as $H_2O$) resides as a minority component within a mixed apolar ice, composed of molecules with a low binding energy (such as CO), the circumstances that would result in the neighbouring CO molecules being sublimated, whilst leaving the $H_2O$ molecules behind are highly contrived. This point was raised in the original study Léger et al. (1985), who suggested that for ices of mixed volatile/non-volatile composition, desorption would probably occur through chemical explosions and posssibly fast spot heating.

It would be very difficult to simulate the co-desorption of different species in models of continuous desorption as the desorption rates will be critically dependent on the ice mantle composition and structure at the time of the heating events.

### 4.4 Application to very small grains

The effects of cosmic ray driven chemistry in cold ices have been shown to be very significant, especially in the formation of complex organic molecules (Shingledecker et al. 2018), but a more direct 'hot' chemistry may be more applicable in the case of very small grains (VSGs), with $a \leq 0.03$ μm. As shown in Bringa & Johnson (2004), grains do not have to be very much smaller than the classical size of

0.1 μm for prompt and thermal spike sputtering processes to become significant. Indeed, for the smallest grains, these processes will dominate and molecular dynamics models suggest there is a strong possibility of refractory core disruption and/or melting (e.g. see fig. 1 of Bringa & Johnson 2004). In addition, the high local electron fluxes and ionizations/dissociations will enhance the desorption efficiency and very possibly drive a rich gas-phase chemistry, perhaps leading to the formation of COMs. For these grains, it is therefore apparent that both the peak temperatures and also the total desorption efficiencies will be higher than the simple scaling laws suggest.

For VSGs the thickness of the ice mantle may be comparable to, or larger, than the refractory cores, in which case the geometrical increase of the surface area of the ice layers must be taken into account. For these grains;

$$N_{\rm CO} \simeq \frac{4\pi}{3}\left(a^3 - a_0^3\right)\frac{N_{\rm i}}{\Delta a}$$

where $a_0$ is the (bare) grain radius, $a = a_0 + n_{\rm L}\Delta a$ is the the radius of the grain with $n_{\rm L}$ layers of ice and $\Delta a$ is the thickness of an ice layer. With the values given in Table 1, for VSGs, we find

$$N_{\rm CO} = 1.13 \times 10^5 \left[(1 + 0.037 n_{\rm L})^3 - 1\right].$$

So, $n_{\rm L}$ =20, 30, and 50 correspond to $N_{\rm CO} = 4.8 \times 10^5$, $0.95 \times 10^6$, and $2.5 \times 10^7$, respectively. This, of course, underestimates $N_{\rm CO}$ as it does not take account of the increased path-length (and hence energy deposition) for cosmic rays passing though grains with relatively thick ice mantles. In fact, if we consider the extreme case of $a_0 \rightarrow 0$, i.e. a pure ice grain, then we can identify an 'ice grain' radius at which the energy deposition is matched by the binding energy of the (assumed pure) ice. This is:

$$a = 0.64\sqrt{f_{\rm ice}/T_{\rm B}^{\rm cool}}$$

where $f_{\rm ice}$ is the energy deposition efficiency ('stopping power') in ice relative to that for refractory grain material. With $f_{\rm ice} \sim 0.5$ and $T_{\rm B}^{\rm cool} = 1200$ K, this gives $a = 0.013$ μm, implying that total mantle desorption will indeed be applicable to the smallest grains in a typical MRN-type distribution. Although this is a very approximate calculation, even if we include the refractory core in this calculation, then we conclude that it is highly likely that for grains with $a \lesssim 0.02$ μm *complete* mantle desorption will occur.

Such processes, which involve bulk/volume sublimation, are hard to quantify by (continuous) surface desorption rates. Total mantle desorption would be equivalent to a continuous desorption injection rate (cm$^{-3}$ s$^{-1}$) of:

$$\dot{n}_{\rm i} = (n_{\rm i})_0/t_{\rm impact},$$

where $(n_{\rm i})_0$ represents the solid-state abundance of species $i$ at the time of the cosmic ray heating event, *and in the absence of the continuous cosmic ray heating desorption*. However, $(n_{\rm i})_0$ is not known in the continuous desorption model, so that we need to consider the chemical processes in individual desorption events to ascertain the significance of whole mantle desorption.

## 5 THE MODEL OF SPORADIC DESORPTION

To understand the implications of the issues that we have raised in the previous section; (a) a true representation of the sporadic desorption, (b) co-desorption of ice mantle species, and (c) total mantle desorption for VSGs, requires a different approach to the continuous desorption approximation that is normally used.

To investigate these issues; most significantly the differences and discrepancies that may occur as a result of representing the sporadic heating and desorption processes by continuous desorption rates we have developed a model that follows the chemical evolution of the gas-phase and gas–grain chemistry through several cosmic ray impact cycles.

The model is based on a simple one-point, dynamically static, application of the STARCHEM model that we have used in other studies (e.g. Rawlings & Williams 2021). For the purpose of our study, we assume that the system is well-evolved and in chemical quasi-equilibrium, which is consistent with our understanding of the conditions within dense cores and pre-stellar star-forming regions (e.g. Rawlings, Keto & Caselli, in preparation). Thus the chemistry is evolved with fixed physical conditions (density, temperature, extinction etc.) with the DLSODE integration package. Note that it is considerably more difficult to construct and apply meaningful models in dynamically evolving systems, particularly those for which the relevant time-scales are short compared to the desorption cycling time-scale.

The model is similar to that applied to other dark cloud environments, the main features of which are as follows: the time-dependent chemistry is followed of some 81 gas-phase and 17 solid-state species, composed of the elements H, He, C, N, O, S, and a representative low ionization potential metal; Na, coupled through a network of 1250 reactions. Reaction data is taken from the UDFA12 data base. The gas-phase, gas-grain (freeze-out and desorption) and surface chemistry (limited to the simple hydrogenation of radicals, reactions involving $O_2$ and some, empirically constrained, $CO_2$ formation from OH/O/$O^+$ impacting bound CO) are all included. However, for the sake of clarity, and to quantify the role of the cosmic ray induced desorption process in determining the gas-phase densities in high density/high extinction regions, most continuous desorption mechanisms (direct and cosmic ray induced photodesorption, species-specific enthalpy-of-formation driven desorption, non-selective desorption driven by $H_2$ formation etc.) have been suppressed in these calculations, with the exception of thermal desorption. The model also calculates, on a continuous basis, the detailed, layer-by-layer composition of the dust grain ice mantles, and also makes due allowance for the geometrical scaling of the grain size and total dust surface area as ice mantles accumulate (so that the nominal bare grain radius is an important parameter); the so-called three-phase model of chemical evolution. Thus, desorption is assumed to only be effective from the surface layer of ice, which includes the partially complete top layer, and any exposed parts of the lower layers. Only the surface layers are treated as being chemically active, and liable to addition or removal. In this simplified model we do not include allowances for grain porosity or the diffusion between layers or account for the possibility of ice melting and the mixing of the layers that may occur as a result of strong heating events.

The (undepleted) elemental abundances are given in Table 1 and are typical of values adopted for low-mass star-forming regions (e.g. van Dishoeck et al. 2021) although, as we are not attempting to model a specific source in this study, the values are not critically important. The chemical initial conditions are taken to be atomic, with the H:$H_2$ ratio set to $10^{-3}$ and we assume that $\gtrsim$90 per cent of the carbon has been converted to CO at the start of the calculations. Other parameters are as specified in Table 1

There are three phases in the models:

(I) Initial conditions are established by evolving the chemistry for a long period of time ($\sim$ 10 Myrs).

(II) The desorption phase, during which there is a rapid return of a fraction of the ice mantle to the gas-phase, following one of the desorption models described below. The time-scales for these

processes are very much smaller than the time-scales of Phases I or III and so the return to the gas-phase is treated as being instantaneous.

(III) The chemistry is followed (again, with static physical conditions) for a period of $t = t_{\rm impact}$, as given by equation (9) after which Phase II is repeated.

Phases II and III are repeated for 5 cycles, or until there are no cycle-to-cycle variations in the abundances.

To investigate the various issues discussed above we have considered several different representations of the cosmic ray desorption process that operate in Phase II, in three variants of our model:

### 5.1 Model 1: continuous desorption

As a benchmark, and for the sake of comparison, we have included models in which the (surface) cosmic ray induced desorption is treated as being continuous and operating throughout all stages of chemical evolution (so that Phase II is effectively absent). This is essentially the same representation as described in HH93 *et seq.* so that for these models we apply the formalism and adopt the parameters used in HH93 scaled, where necessary, for different grain sizes/size distributions.

We have considered three variations of this model: for Model 1a, we use the same binding energies and desorption rates as given in HH93, and do not impose the upper limits to the rates as described in the previous section. This is therefore a nearly exact simulation of the HH93 model. For this reference model, we adopt all other parameters as used by HH93 for classical ($a = 0.1\,\mu$m) grains and use desorption rates as determined by the formulae above.

In general, we can scale the cooling time-scale, as used in HH93, for an arbitrary grain size:

$$t_{\rm cool} = 10^{-5}\left(\frac{0.1\,\mu{\rm m}}{a}\right)\exp\left[T_{\rm b}^{\rm cool}\left(\frac{1}{T_{\rm peak}}-\frac{1}{70.84}\right)\right],$$

where $T_{\rm B}^{\rm cool}$ is the binding energy (in K) of the coolant species. Again, note that this is a function of the grain size, both explicitly in the $(1/a)$-dependence and implicitly in the size-dependence of the peak dust grain temperature and hence the (single molecule) evaporation time-scale.

For Models 1b and 1c we use the desorption rates calculated with extended cooling, as discussed and calculated in the previous section, and we also set the upper limits to the desorption rates using equation (11). In Model 1b, we adopt a single nominal grain size of 0.1 μm, whilst in Model 1c we use the desorption rates averaged over an MRN grain size distribution. The rates for the key species are given in Table 3 for both models.

For the other models described below, the continuous cosmic ray induced desorption is replaced by one of the sporadic desorption mechanisms in Phase II, with no desorption (other than thermal desorption) operating in either of Phases I or III.

### 5.2 Model 2: sporadic, species-specific desorption

In this model we assume sporadic, stochastic desorption. That is to say, there is (an assumed instant) injection of each species immediately after a cosmic ray impact/heating event. This is therefore closer to the 'true' situation than the continuous desorption simplification employed in HH93 and Model 1. For clarity, we have again assumed a single 'classical' (0.1 μm) grain size.

Following other studies, in this model we assume that the thermal desorption characteristics of each species are defined for pure ices and are independent of the chemical/physical environment of the desorbing molecules. Therefore, for the purpose of this model (only) we have assumed that – as in the HH93 model – the composition of the ice is homogeneous, i.e. there are no compositional variations in the various ice layers. This is obviously a major simplification but, if we were to adopt a microscopic layer-by-layer approach to the ice composition (as in our other models), then the inconsistencies due to differential desorption as discussed in Section 4.3 would be evident. For the order-of-magnitude type of calculations that we are considering in this model the assumption of a homogeneous ice composition is therefore more workable and is acceptable for our purposes.

The desorption rates derived from the extended cooling calculations are used to determine the number of atoms/molecules of each species that are released into the gas-phase. Thus, the incremental change to the gas-phase fractional abundance of species *i* is given by

$$\Delta X_{\rm i} = k^{\rm i}_{\rm evap}.t_{\rm cool}.\sigma_{\rm H}N_{\rm s}F_{\rm i} = k^{\rm i}_{\rm crd}.t_{\rm impact}.\sigma_{\rm H}N_{\rm s}F_{\rm i},$$

where $k^{\rm i}_{\rm crd}$ are the equivalent cosmic ray induced desorption rates, calculated as described in Section 4.2 above. $F_{\rm i}$ is the (bulk) fraction of the ice mantle that is composed of species *i* which, in this model, is identical to the fractional surface coverage of the species, $f_{\rm i}$. The incremental desorption, so calculated, is subject to the obvious constraint that the number of molecules desorbed per heating event cannot exceed the total initial number of molecules in the ice (i.e. $\Delta X_{\rm i} \le X_{\rm i(ice)}$).

### 5.3 Model 3: Sporadic co-desorption

The other extreme to the species-specific desorption adopted in Model 2 is to assume that the desorption process does not discriminate between different species, so that a single common binding energy applies to *all* surface species. This corresponds to the case of complete co-desorption of ice species. This is, of course, highly speculative and will depend on a number of unknown factors, such as the degree of compositional segregation within ice layers but is, to some degree, guided by laboratory evidence. To simulate this in the model we assume that complete layers, or a fraction of a layer, of ice are completely sublimated without consideration of the compositional variations within those layers. To determine the number of layers that are sublimated, we can use the same formalism as employed in the previous section; simply equating the total sublimation energy with the energy that is required to cool the grain. This model is, again, a huge oversimplification but, together with Model 2, it serves to demonstrate the range of desorption efficiencies that may be possible.

For the calculations presented here we assume that $T_{\rm B}^{\rm i} = T_{\rm B}^{\rm cool} = 1210\,$K, equal to the binding energy for CO in the HH93 model. Whilst this 'common binding energy' is ill-defined it should be noted that, with this formalism, uncertainties in its value will only result in variations in the desorption efficiencies of order unity.

Obviously, for this model, the actual desorption that occurs in each cycle depend on the composition of the surface layers and so the compositional structure of the ices is very important. We consider two scenarios:

(a) Desorption from 'classical' (0.1 μm) grains, for which a limited number of ice layers will be sublimated as described above, and

(b) Desorption from VSGs (0.01 μm), for which complete mantle sublimation, of all ice layers, occurs – as discussed in Section 4.4.

For Model 3(a), the derived desorption rate for species with a binding energy of ∼1100–1200 K from 'classical' grains with

**Table 6.** Description of the models.

| Model | Desorption |
|---|---|
| Model 1a | Continuous, HH93 rates |
| Model 1b | Continuous, extended cooling, $a = 0.1$ μm |
| Model 1c | Continuous, extended cooling, MRN-averaged |
| Model 2 | Sporadic, evaporative cooling |
| Model 3a | Sporadic, co-desorption of top 3 ice layers |
| Model 3b | Sporadic, total ice desorption for VSGs ($a = 0.01$ μm) |

$a = 0.1$ μm corresponds to the complete desorption of the top ∼3 layers of the ice, which is what we have adopted for the model.

### 5.4 Model parameters

For each of our models, calculations have been performed for two representative gas densities and extinctions; (i) $n = 10^5$ cm$^{-3}$, $A_v = 10$, and (ii) $n = 10^7$ cm$^{-3}$, $A_v = 50$; which are typical of values within prestellar dark cores. As we have justified above, for most models the calculations have been performed for 'classical' ($a = 0.1$ μm) grains, for ease of comparison with previous studies. Model 1b is for an averaged MRN grain size distribution and Model 3b is for VSGs ($a = 0.01$ μm). Where $a = 0.1$ μm, the interval between cosmic ray impacts is $t_{impact} = 1.0$ Myr, whereas for $a = 0.01$ μm, $t_{impact} = 100.0$ Myr. The energy deposition per cosmic ray impact is taken to be proportional to the grain size, $a$.

Of course, these models determine the time-dependences of the chemical abundances (gas-phase and solid-state) for a single representative grain through one impact/cooling cycle. To ascertain the significance of cosmic ray induced desorption in astrochemical models we obviously need to obtain the mean abundances for a system containing many grains at different phases of the cycle. We therfore determine statistical averages of both the gas-phase and solid-state abundances by calculating the (time-averaged) mean values over individual cycles. The key characteristics of the models are given in Table 6 and the values of other parameters are as specified in Table 1.

## 6 MODEL RESULTS

In this section, we present the results from the models as plots of the abundances of key species as a function of time for each of the five studied desorption cycles, and as the numerical time-averaged values of the abundances for the final (∼equilibrium) cycle. We have considered the chemical evolution following the impact(s) of cosmic rays on a single, representative, grain. However, the time-averaged values of the abundances in the limit cycle are effectively representative of the mean values of the abundances in an ensemble of grains at different stages within the heating and desorption cycle. This is, of course, subject to the limitation that we are considering a single, or in some cases population-averaged, value of the grain size and a single cosmic ray energy, but does serve to show the effects in macroscopic objects. We must also make it clear that these results have been obtained for a rather specific physical model with somewhat contrived chemical constraints and are not generic. As such, and unlike the the more rigorous discussion in Section 4, they must be considered indicative, rather than definitive.

First, in Fig. 1 we show the composition of the ice mantles as determined at the end of Phase I and for the case of grains of radius $a = 0.1$ μm and a gas density of $n = 10^5$ cm$^3$. Abundances are shown as a function of monolayer, so that the values on the right-hand side of this plot give the composition of the outermost (surface) layer.

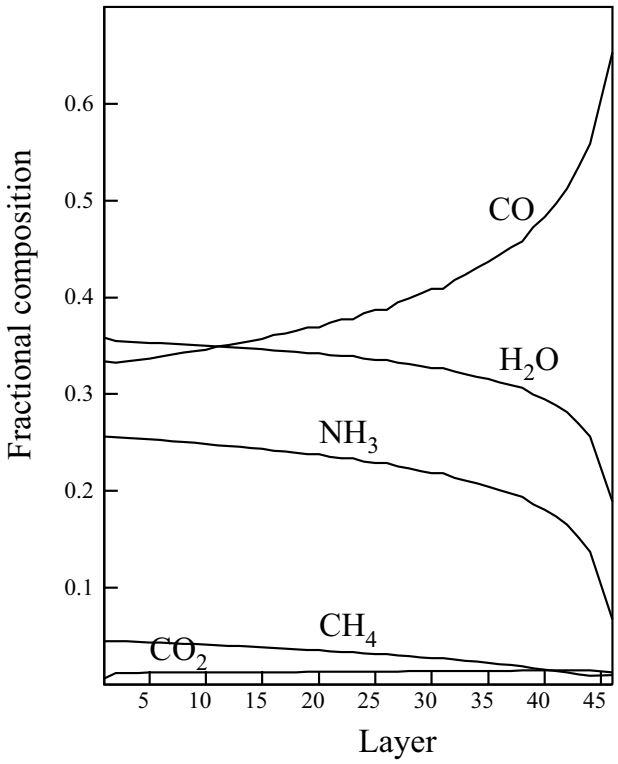


**Figure 1.** Ice mantle composition as a function of monolayer number, for models with a $= 0.1$ μm and $n = 10^5$ cm$^{-3}$.

From this figure we can see that, for the conditions that we have investigated in this study, the composition of the outer 5–10 layers of the ice mantles is dominated by CO. The surface layers are composed of CO (∼70 per cent) and $H_2O$ (∼20 per cent) with other species (e.g. $NH_3$, $CH_4$, and $CO_2$) accounting for the remaining 10 per cent. Deeper into the ice (i.e. for the inner 25 layers), the composition is much more heterogeneous. In our model, we have adopted somewhat arbitrary physical and chemical conditions: we follow the chemical evolution and ice formation whilst keeping the physical parameters (such as the density and temperature) static, and exclude all desorption mechanisms, other than thermal desorption and cosmic ray induced desorption. Making these assumptions, we find that the ice mantle composition as shown in this figure is fairly insensitive to the assumed mean grain size and gas density (over the ranges $0.01\ \mu m < a < 0.1\ \mu m$, $10^5\ cm^{-3} < n < 10^7\ cm^{-3}$). This will almost certainly not be the case for more realistic chemical/dynamical simulations. However, for our models, this justifies *a posteriori* the simplification made above that we can adopt a single species (CO) and binding energy for the grain cooling calculations.

Fig. 2 shows the time-dependence of several key gas-phase species for each of the five cycles in the cases of Model 2 (sporadic desorption; Fig. 2a) and Model 3a (sporadic co-desorption; Fig. 2b). From this figure, we can see that the modelled gas-phase chemical abundances are clearly different for the two models so that, for example, $NH_3$ is very efficiently produced in Model 2 (sporadic desorption) whereas the co-desorption in Model 3a results in strong enhancements of the more tightly bound species, such as $H_2O$ and $H_2S$. We can also see that the chemical behaviours can be quite complex and that we need to consider the time-averaged abundances in each cycle to obtain a meaningful understanding of the chemical

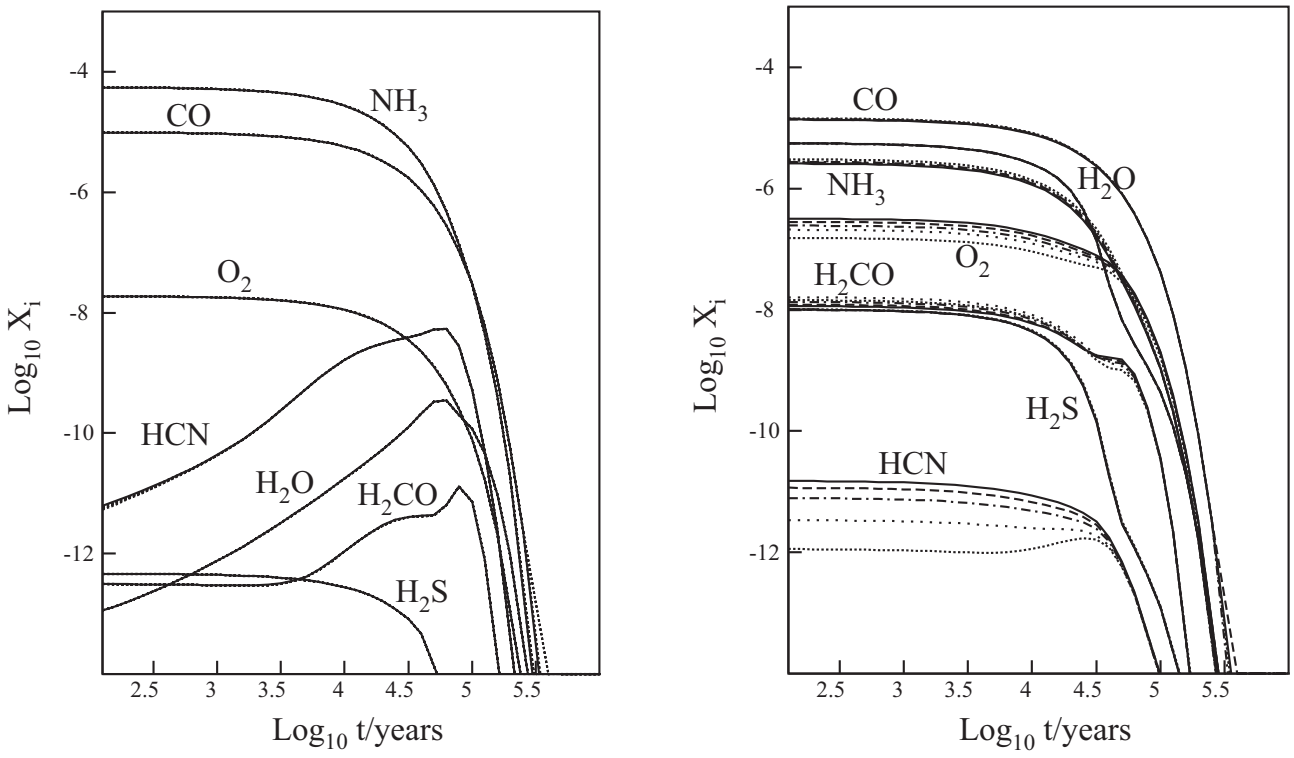


**Figure 2.** Results from Models 2 (lhs) and 3a (rhs), with $a = 0.1$ μm, $n = 10^5$ cm$^{-3}$: Fractional abundances of selected species are shown as a function time since the cosmic ray heating event for the first five impact cycles. For Model 3a, the logarithmic abundances of HCN have been lowered by 4 for the sake of clarity. The solid lines show the results for the final (fifth) cycle, whilst the results from the previous cycles are shown by the close dotted (cycle 1), wide dotted (cycle 2), dashed–dotted (cycle 3) and dashed (cycle 4) lines.

trends. The behaviour of $H_2O$ (and HCN) in Fig. 2a is particularly interesting; the desorption of these species is minimal, yet they experience strong second-order transient enhancements that are driven by the enriched gas-phase chemistry.

It is also apparent that, for the particular values of the free parameters used in these models, there are very little cycle-to-cycle variations in the abundance profiles (except for Model 3a in the case of HCN and, to a lesser extent, $NH_3$). This is primarily a consequence of the fact that the gas-phase and freeze-out time-scales are relatively short compared to the interval between cosmic ray impacts ($t_{\rm impact}$), so that the transient chemical effects of the desorption in one cycle are 'lost' before the next cycle starts.

Table 7 presents the time-averaged gas-phase abundances of selected species for each of the models described above, for the final (fifth) cycle of the calculations. Results are shown for each of the desorption models (Models 1–3) for an environment in which the density is $10^5$ cm$^{-3}$ and the visual extinction is 10 mag. Table 8 shows the results (with the same format as Table 7) for a higher density ($10^7$ cm$^{-3}$) and darker ($A_{\rm v} = 50$) environment.

Comparing the results for the continuous desorption model with extended cooling (Model 1b) to the reference model (Model 1a) we can see that, for the low density case, the differences are mostly fairly minimal (although non-negligible in the cases of $CH_4$, $H_2CO$, and HNO) indicating that continuous CR-induced desorption is not critical in defining the chemistry in these environments. In contrast, for the higher density case, the abundances are typically enhanced by a factor of ∼10 or more – as expected. Extending the model from a single size (0.1 μm) population to an average over an MRN-type size distribution (Model 1c) results in strong enhancements of the more tightly bound species (such as $H_2CO$, and the sulfur species) and these are particularly significant in the high density case. Such effects are a consequence of the strong contributions from the smaller grains, that are heated to higher temperatures by cosmic ray impacts. The differences between the sporadic desorption model (Model 2) and the continuous desorption model (with extended cooling; Model 1b) are mostly fairly minor – due to the relatively short chemical time-scales for the adopted model parameters, as discussed above. However, there are a few notable differences for the low density calculations (only); importantly, Model 2 results in large enhancements of CO, $NH_3$, and HNO (by factors of ∼10, ∼41, and ∼24, respectively).

The (non-species-specific) co-desorption model (Model 3a) results in very strong enhancements, by factors of ∼10–100, for nearly all species (other than $CH_4$ and $NH_3$). This is particularly acute in the cases of those that have small, yet significant, abundances in the ices – such as $H_2O$, $CO_2$, and the sulfur species – which are enhanced by several orders of magnitude. As with the other models, the trends tend to be amplified in the high density calculations, although not for CO, $CH_4$, $NH_3$, $N_2$, or $O_2$.

The model specific to total mantle desorption from VSGs, with $a = 0.01$ μm (Model 3) again results in big changes to the abundances but, whilst some (such as $H_2O$, $CO_2$, and the sulfur species) are very strongly enhanced – by several orders of magnitude in the high density calculations – the more volatile species ($CH_4$, $NH_3$, $N_2$, $O_2$, HCN, HNC, and even CO in the high density case) actually have lower abundances than those determined in the extended cooling continuous desorption model (Model 1b). This indicates that a degree of chemical differentiation may occur in those situations where a large population of small grains dominates the desorption.

As noted above the chemical effects of the desorption are mostly self-contained within each cycle and the changes on longer

**Table 7.** Model results (low density; $n = 10^5$ cm$^{-3}$, $A_v = 10$): time-averaged fractional abundances of selected species for the final cycle. For $H_2O$, results are given for two values of the binding energy (see Section 4.2 for details).

| Species | Model 1a | Model 1b | Model 1c | Model 2 | Model 3a | Model 3b |
|---|---|---|---|---|---|---|
| CO | 1.8(−8) | 2.0(−8) | 2.5(−8) | 2.0(−7) | 2.7(−7) | 1.6(−8) |
| $H_2O$ | 3.6(−11) | 3.8(−11) | 4.7(−11) | 2.3(−11) | 6.9(−8) | 1.1(−8) |
| $H_2O^\dagger$ | 3.6(−11) | 3.8(−11) | 8.0(−11) | 2.8(−11) | 6.9(−8) | 1.1(−8) |
| $CH_4$ | 4.7(−10) | 4.5(−9) | 5.1(−9) | 1.1(−9) | 1.2(−8) | 1.1(−9) |
| $NH_3$ | 1.1(−8) | 2.1(−8) | 2.7(−8) | 8.6(−7) | 3.5(−8) | 7.3(−9) |
| $N_2$ | 4.7(−10) | 5.7(−10) | 7.9(−10) | 2.5(−9) | 6.4(−9) | 8.5(−11) |
| $O_2$ | 2.9(−10) | 1.4(−10) | 2.3(−10) | 4.0(−10) | 7.6(−9) | 1.4(−11) |
| $H_2CO$ | 1.2(−12) | 6.1(−12) | 9.2(−12) | 7.8(−13) | 2.4(−10) | 5.3(−12) |
| $CO_2$ | 7.7(−14) | 9.4(−14) | 2.9(−13) | 2.1(−13) | 9.8(−9) | 6.3(−10) |
| HCN | 2.0(−11) | 5.7(−11) | 1.2(−10) | 3.7(−10) | 3.1(−9) | 2.4(−11) |
| HNC | 2.3(−11) | 6.4(−11) | 1.2(−10) | 4.8(−10) | 2.3(−9) | 2.7(−11) |
| HNO | 1.7(−12) | 9.4(−12) | 2.3(−11) | 2.3(−10) | 2.0(−9) | 2.0(−11) |
| $H_2S$ | 4.3(−16) | 8.4(−16) | 2.9(−14) | 9.1(−15) | 1.2(−10) | 1.3(−11) |
| $C_2S$ | 2.1(−25) | 4.8(−25) | 6.4(−21) | 5.7(−24) | 1.2(−16) | 3.6(−16) |
| HCS | 2.7(−19) | 9.6(−19) | 7.5(−17) | 1.9(−18) | 2.0(−12) | 1.0(−13) |

**Table 8.** Model results (high density; $n = 10^7$ cm$^{-3}$, $A_v = 50$): time-averaged fractional abundances of selected species for the final cycle. For $H_2O$, results are given for two values of the binding energy (see Section 4.2 for details).

| Species | Model 1a | Model 1b | Model 1c | Model 2 | Model 3a | Model 3b |
|---|---|---|---|---|---|---|
| CO | 3.1(−10) | 2.7(−9) | 2.2(−9) | 2.0(−9) | 2.9(−9) | 1.6(−10) |
| $H_2O$ | 9.1(−16) | 8.6(−15) | 6.9(−15) | 2.5(−16) | 9.3(−10) | 1.1(−10) |
| $H_2O^\dagger$ | 8.2(−15) | 2.5(−14) | 8.2(−13) | 4.6(−14) | 9.3(−10) | 1.1(−10) |
| $CH_4$ | 4.7(−13) | 6.9(−12) | 6.8(−12) | 1.1(−11) | 3.6(−11) | 1.1(−11) |
| $NH_3$ | 2.0(−10) | 3.7(−9) | 3.5(−9) | 9.0(−9) | 5.3(−10) | 7.3(−11) |
| $N_2$ | 1.8(−12) | 1.3(−11) | 1.1(−11) | 8.1(−12) | 1.7(−11) | 4.3(−13) |
| $O_2$ | 9.5(−14) | 8.1(−13) | 6.4(−13) | 6.0(−14) | 5.8(−13) | 2.3(−15) |
| $H_2CO$ | 2.0(−17) | 8.8(−17) | 1.3(−15) | 1.1(−17) | 2.4(−13) | 2.6(−15) |
| $CO_2$ | 1.8(−19) | 3.8(−18) | 1.8(−15) | 1.3(−18) | 8.0(−11) | 6.1(−12) |
| HCN | 6.3(−16) | 1.6(−14) | 2.7(−14) | 9.8(−15) | 4.3(−12) | 5.7(−14) |
| HNC | 2.3(−15) | 5.0(−14) | 5.9(−14) | 6.5(−14) | 2.8(−12) | 2.9(−14) |
| HNO | 2.9(−16) | 2.8(−15) | 5.5(−15) | 1.3(−15) | 1.2(−13) | 4.6(−16) |
| $H_2S$ | 5.2(−17) | 1.2(−16) | 3.7(−15) | 1.0(−16) | 2.5(−12) | 1.3(−13) |
| $C_2S$ | 1.6(−25) | 1.8(−25) | 2.5(−21) | 1.0(−25) | 9.2(−17) | 6.0(−18) |
| HCS | 7.4(−20) | 1.3(−19) | 2.2(−17) | 3.6(−20) | 4.8(−14) | 6.2(−16) |

time-scales are mostly fairly marginal. Hence, the similarity between the results obtained with the sporadic and the continuous desorption formalisms. Whilst this is as expected when $t_{impact}$ greatly exceeds the chemical time-scales, this will not be the case if the time-scales are comparable (e.g. if the gas density is lower, or the cosmic ray ionization rate, $\zeta$ is higher). To illustrate this we have run Model 2 with $\zeta = 5 \times 10^{-16}$ s$^{-1}$ (for $a = 0.1$ μm, $n = 10^5$ cm$^{-3}$, and $A_v = 10$), and the results are shown in Fig. 3 and Table 9. These are clearly very different to what was obtained with the lower value of $\zeta$; the relative abundances are strongly modified (and in fact are closer to what was obtained for Model 3). Most importantly, they show that the shorter interval between desorption events leads to chemical variations in one cycle being carried forward to the next cycle. This is quantified in Table 9, which gives the mean abundances in each of the five desorption cycles. From this we can see that, relative to Table 7, the abundances of most species are enhanced by at least two orders of magnitude and, in some cases, significantly more. This is particularly important in the cases of CO and, especially, $H_2O$ where the transient enhancements discussed above are transmitted from cycle to cycle. Significant (and in some cases non-monotonic) cycle-to-cycle variations for most species are also evident; whilst the abundances of some species decline (e.g. $H_2O$, $NH_3$, $O_2$, HCN, HNC, and $H_2S$), the abundances of others rise (e.g. $HCO^+$, $N_2$, and $N_2H^+$). The cycle-dependence is particularly dramatic in the cases of $NH_3$ and $O_2$, for which the mean abundances both decline by a factor of ∼100 from cycle 1–5.

Although the cycle duration is much shorter, five cycles (after which cycle-to-cycle chemical equilibrium has still not been established) corresponds to a time interval of 0.13 Myr. It is therefore quite obvious that the continuous desorption representation breaks down in these circumstances and that this situation is one that would be very hard to quantify and apply to standard astrochemical models.

## 7 COMPARISON WITH OTHER STUDIES

The various issues that we have discussed in this work (extended cooling lifetimes, a corrected model of the application to interstellar grain size distributions, treatment of the desorption process as sporadic, as opposed to continuous, the possibility of species co-desorption and whole mantle evaporation from very small grains)

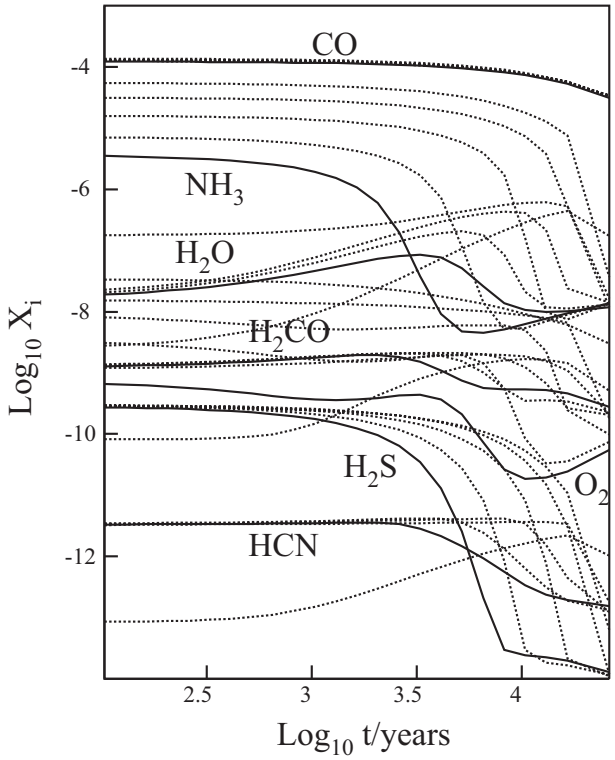


**Figure 3.** Results from Model 2, with an enhanced value of $\zeta$ ($5 \times 10^{-16}$ s$^{-1}$), for $a = 0.1$ μm, $n = 10^5$ cm$^{-3}$, and $A_v = 10$: Fractional abundances of selected species are shown as a function time since the cosmic ray heating event for the first five impact cycles. The logarithmic abundances of $O_2$, HCN, $H_2CO$, and $H_2S$ have been lowered by 2, 6, 2, and 2, respectively, for the sake of clarity. The solid lines show the results for the final cycle, with results from the previous cycles shown by the dotted lines.

**Table 9.** Results from Model 2 with an enhanced cosmic ray ionization rate ($\zeta = 5 \times 10^{-16}$ s$^{-1}$): time-averaged fractional abundances of selected species for the first 5 desorption cycles.

| Species | Cycle 1 | Cycle 2 | Cycle 3 | Cycle 4 | Cycle 5 |
|---|---|---|---|---|---|
| CO | 7.9(−5) | 7.6(−5) | 7.5(−5) | 7.4(−5) | 7.2(−5) |
| $H_2O$ | 2.8(−7) | 4.2(−7) | 1.9(−7) | 6.1(−8) | 2.5(−8) |
| $NH_3$ | 2.0(−5) | 8.9(−6) | 2.9(−6) | 6.8(−7) | 2.0(−7) |
| $O_2$ | 1.1(−6) | 8.1(−7) | 3.2(−7) | 6.3(−8) | 1.2(−8) |
| $HCO^+$ | 2.0(−9) | 3.3(−9) | 4.8(−9) | 6.1(−9) | 7.1(−9) |
| $H_2S$ | 7.4(−9) | 6.7(−9) | 4.8(−9) | 3.1(−9) | 2.1(−9) |
| HCN | 1.6(−6) | 3.0(−6) | 2.2(−6) | 1.4(−6) | 9.3(−7) |
| HNC | 1.3(−6) | 2.4(−6) | 1.8(−6) | 1.1(−6) | 7.2(−7) |
| $N_2$ | 6.7(−6) | 1.1(−5) | 1.5(−5) | 1.8(−5) | 1.9(−5) |
| $N_2H^+$ | 9.2(−11) | 2.2(−10) | 3.9(−10) | 5.2(−10) | 6.1(−10) |

have not been discussed in any detail in previous studies, which makes direct comparison difficult. However, it is useful to place this work in the context of these other studies and to identify the sources of uncertainty, where known.

There have been several recent studies of cosmic ray induced desorption in the literature. Some studies have addressed the physics of the interaction between the cosmic ray particles and the dust grains, e.g. Ivlev et al. (2015a) considered a model of localized spot-heating driven explosions, whilst Kalvāns & Kalnin (2020a) is the only other investigation that has considered the time-dependence of the coupled cooling, and layer-by-layer evaporative cooling of different molecular species. That study tracked the cooling profile, the composition of the ices and the evaporative yields for several species. However, it did not determine the effective desorption rates or consider the chemical effects on an environment that is subject to repeated heating and desorption events. Kalvāns & Kalnin (2020b) extended the study to include the effects of variations in the grain heat capacity and also concluded that the desorption is most efficient for small grains, with CO desorption dominated by grains with $a <$ 0.05 μm.

As stated above, for the reasons given, we have conducted our study within, and extending, the paradigm stated in HH93 – centred on a study of the sporadic heating of 0.1 μm grains to a peak temperature of ∼70 K, at the rate of one event per Myr. In reality, there will be a spectrum of cosmic rays of varying composition and stopping power impacting grains of varying composition and structure. Furthermore, the relationship between these parameters and the cosmic ray energy/flux is not necessarily linear (e.g. see equation 16 of Léger et al. (1985), implying that – for a given grain size – there will be a spectrum of values for $T_{peak}$ and $t_{impact}$). Other studies have therefore concentrated more on taking the standard whole grain heating, continuous desorption, model and adapting it for a range of grain sizes, ice mantle thicknesses and cosmic ray energy spectra, including any attenuation effects that may be appropriate. Thus, Kalvāns (2016) extended the HH93 model to consider the effects of a spectrum of cosmic rays on grains of bare radius 0.05–0.2 μm and varying ice thickness in a translucent cloud ($A_v = 2$). They found that $t_{impact}$ may be overestimated by two orders or magnitude or more, particularly for low-energy impacts resulting in $T_{peak} \sim$ 20–30 K. This is probably too low to effect efficient desorption, but can promote surface chemistry. Zhao et al. (2018) investigated the dependence of the desorption rates on grain size and found that the differential depletion of volatile species is sensitive to the population of large grains ($> 0.1$ μm) that are heated to lower temperatures, although – as discussed in Section (3) – this finding was based on an erroneous definition of the grain cooling time-scale. This was also used by Sipilä et al. (2020) who determined the dust grain equilibrium temperatures resulting from CR impact heating; which have important effects on the thermal diffusion and surface reaction rates for solid-state species. In that study they investigated the dependence of the desorption efficiencies on the grain size and found that the desorption rate is weighted towards the larger grains in a normal interstellar size distribution. Kalvāns & Kalnin (2019) considered the chemical effects of a spectrum of cosmic rays resulting in a range of values for $T_{peak}$ and $t_{impact}$. The results are presented in the context of a specific physical evolutionary model of a contracting dense core. This study also gives analytical relationships between $T_{peak}$ and $t_{impact}$, as well as their dependence on the extinction ($A_v$).

Sipilä et al. (2021) emphasized how the desorption efficiency depends on the structured content of the different layers of the ices, but made the assumption that the binding energies are well-defined for each species and not dependent on their environment. In their model, the cooling (but not the temperature-dependences of the desorption rates themselves) was treated time-dependently. A cosmic ray energy/flux spectrum was used to determine $t_{impact}$, but the complexities of the situation are apparent in that $t_{impact}$ depends on a variety of factors including the shape and strength of the cosmic ray spectrum, the nature of the particles, the depth-dependence of the attenuation of the flux and how that varies as a function of the energy, and hence the depth-dependence of the dust opacity and the grain size distribution. Silsbee et al. (2021) have presented a very complex model which describes desorption as a function of the size and composition of both the core grain and the ice mantle,

**Table 10.** Results from Model 2 for selected species, with $T_{peak} = 54$ K and $t_{impact} = 10^{11}$ s. The second column gives the desorption rate ($s^{-1}$), and columns 3–6 give the mean (cycle-averaged) fractional abundances after 1, 10, 20, and 100 cycles, respectively. For $H_2O$, results are given for two values of the binding energy (see Section 4.2 for details).

| Species | $k_{54}$(0.1 μm) | Cycle 1 | Cycle 10 | Cycle 20 | Cycle 100 |
|---|---|---|---|---|---|
| CO | 1.3(−11) | 4.3(−6) | 2.2(−5) | 2.4(−5) | 1.4(−5) |
| $CH_4$ | 6.1(−13) | 1.4(−8) | 7.2(−8) | 1.0(−7) | 1.2(−7) |
| $H_2O$ | 2.1(−41) | 8.2(−10) | 8.3(−8) | 2.2(−7) | 2.4(−8) |
| $H_2O^{\dagger}$ | 2.5(−17) | 8.3(−10) | 8.3(−8) | 2.2(−7) | 2.4(−8) |
| $NH_3$ | 2.1(−10) | 2.6(−5) | 2.8(−5) | 1.7(−5) | 9.6(−8) |
| $N_2$ | 1.3(−11) | 3.4(−7) | 3.7(−6) | 5.4(−6) | 3.6(−6) |
| HNC | 2.1(−14) | 1.7(−8) | 6.7(−7) | 1.0(−6) | 1.5(−7) |
| $H_2CO$ | 1.4(−16) | 2.1(−12) | 8.9(−10) | 3.3(−9) | 1.6(−8) |

**Table 11.** Time-averaged fractional abundances of selected species for models in which all desorption mechanisms are included ($n = 10^7$ cm$^{-3}$, $A_v = 50$). See text for details.

| Species | Reference | Model 1c | Model 2 | Model 3a |
|---|---|---|---|---|
| CO | 8.9(−11) | 1.7(−9) | 2.3(−9) | 2.1(−9) |
| $H_2O$ | 3.2(−11) | 3.4(−11) | 3.2(−11) | 2.0(−9) |
| $NH_3$ | 6.0(−13) | 1.1(−9) | 7.3(−9) | 4.9(−11) |
| $HCO^+$ | 8.6(−14) | 1.6(−12) | 1.1(−13) | 1.2(−13) |
| $CO_2$ | 7.4(−12) | 8.2(−12) | 3.2(−12) | 1.1(−10) |
| HCN | 2.6(−15) | 9.1(−15) | 1.4(−14) | 1.3(−13) |
| $N_2$ | 1.2(−11) | 1.9(−10) | 1.5(−10) | 2.9(−10) |

and includes a cosmic ray transport model with a depth-dependent spectrum. They found that there are strong variations of the ice mantle thickness with grain size.

Taking these various issues together, this is potentially a very complicated problem to solve; even if the nature and energy transport of the cosmic rays were known, there are additional uncertainties in the microphysics; in the WGH model the rate of thermal diffusion within the grains depends on their composition, shape and structure/porosity, whilst the desorption rates will be moderated by the fact that there will be grain size- and source-specific variations in the compositional structure of the ice mantles.

There are clearly a large number of factors and a wide range of the key physical parameters ($T_{peak}$, $t_{impact}$ etc.) that need to be investigated further using the results from our study. However, a key feature of most of these studies is that, by considering the spectrum of cosmic rays, heating events (leading to low values of $T_{peak}$) occur much more frequently than once every 1 Myr – possibly by a factor of 100× or more. This introduces additional complexity as the lower peak temperatures will result in increased segregation between the desorption efficiencies of volatile and non-volatile species. Most significantly, the discrepancies between the sporadic and the continuous desorption approaches will be evident and must be considered.

For the purpose of comparison, a useful compromise and simplification is given by Kalvāns (2021) who identify a single, weighted mean, value of 54 K for $T_{peak}$ and a simple analytical dependence of $t_{impact}$ on the hydrogen column density. We have tested this in our Model 2 (sporadic desorption) with $A_v = 10$ and density $10^5$ cm$^{-3}$ (as for the models of low-density regions discussed above), for which the implied period between impacts is $t_{impact} = 10^{11}$ s. Other parameters are as given in Table 1, as before.

The results, given in the form of the mean cycle-averaged fractional abundances of several gas-phase species, are shown in Table 10. These demonstrate that, for these parameters (and particularly due to the much lower value of $t_{impact}$), the behaviours are similar to the case that we investigated above for $\zeta = 5 \times 10^{-16}$ s$^{-1}$, in that the chemical evolution of individual desorption cycles are not independent of each other and the abundances of most species (including CO and $H_2O$) are very significantly enhanced. The table shows how these variations can be carried over after many tens of cycles. These changes are especially noticeable in the case of $NH_3$, whose mean abundance falls by a factor of >170 between cycles 20 and 100. Indeed, these variations are still evident and an equilibrium 'limit cycle' has still not been established even after 100 cycles (i.e. ∼0.3 Myr).

## 8 DISCUSSION AND CONCLUSIONS

In this study we have extended and developed models of the cosmic ray heating induced desorption of species from ice mantles to include: a description of the grain cooling and desorption profiles, a revised analysis of grain size population-averaged rates, consideration of upper limits to the rates, set by the availabilities within the ice mantle, treatment of the process as being sporadic, rather than continuous, the possibility of species co-desorption, and whole mantle desorption from very small grains.

We do not make any claims to be definitively accurate in quantifying the cosmic ray induced desorption rates. However, this study is based on the energetics of the process; balancing the heating rate by the energy lost through the evaporative cooling of the ice constituents. Because of this, our results are reasonably robust to any assumption concerning the precise nature of the desorption mechanism and the uncertainties in the microphysics of the interactions between the cosmic ray particles and dust grains. Using the conservation of energy approach, the only controlling parameters in the determination of the desorption rates are (i) the mean energy deposited in a grain per cosmic ray impact ($\Delta E$), (ii) the mean interval between cosmic ray impacts ($t_{impact}$), and (iii) the binding energies of the atomic and molecular species in the dust ice mantles ($E_B^i$). Unfortunately, these are all ill-defined so that there are significant uncertainties in the derived desorption rates.

Compared to previous studies, which are based on a continuous representation of the cosmic ray induced desorption process, the two overarching conclusions of this study are that (a) the cosmic ray induced desorption rates are highly uncertain, and (b) they have almost certainly been underestimated – and possibly particularly so for the more tightly bound species, such as $H_2O$.

Whatever model we adopt there are huge uncertainties (possibly by orders of magnitude) due to the poor constraints on the many free parameters, some of which were highlighted in the previous section. It is therefore currently inappropriate to make any specific astrochemical deductions. Indeed, it may therefore be necessary to 'invert' the problem and to use observationally deduced molecular abundances in dense regions (with reasonably well-defined physical conditions) to infer the desorption rates.

Specifically, our findings are that:

(i) Cosmic ray induced desorption rates are almost certainly very much larger than the values that have been adopted in most previous studies. Even within the simple paradigm of HH93 (a single grain size, impacted by cosmic rays of the same energy/composition with a single time interval between impacts) a realistic representation of the cooling/desorption profiles indicates that the desorption rates (especially those of the more volatile species) should be $\gtrsim 10\times$ larger. Generally, the significance of this is only apparent at higher densities

($\gtrsim 10^5$ cm$^{-3}$), where the role of cosmic ray induced desorption is more significant.

(ii) A consideration of the dependences of the heating rates, peak dust grain temperatures and the cooling rates for grains of different sizes shows that, for grain size distribution typical of the ISM, desorption from the smallest grains dominates. This is different to what has found in previous studies, which have used a different definition of the grain cooling time-scale. The small grains will achieve higher peak temperatures than the classical 0.1 μm grains so that the most important effect of this is that the desorption rates for the more tightly bound species are significantly enhanced.

(iii) Desorption rates are limited by the availability of the desorbed species within the ice mantles. In practice, this is equivalent to saying that, using the HH93 formalism and parameters, $k^{\rm i}_{\rm crd} < 10^{-12}$ s$^{-1}$.

(iv) The combined effect of the points highlighted above is to result in a somewhat compressed dynamic range for $k^{\rm i}_{\rm crd}$. Recognizing that the binding energies of molecular species in ices are highly uncertain (especially in the case of mixed composition ice) we have provided a table of the desorption rates (for both the 'classical' 0.1 μm grains and for an MRN-weighted distribution of grain sizes) as a function of binding energy. This data can easily be incorporated into astrochemical models.

(v) If we do *not* make the usual assumption that the sporadic/stochastic mechanism of cosmic ray impacts/heating/desorption can be represented as a continuous but instead follow the chemical evolution through successive heating and desorption cycles; we obtain similar results for most species (but not all; most notably there are large differences for CO and $NH_3$) – but *only* if the desorption cycles are chemically independent of each other. However, the discrepancies between the sporadic and the continuous representations become significant when the interval between cosmic ray impacts is shorter than the chemical time-scales. The key time-scale here is that for freeze-out so that, using the HH93 description for 0.1 μm grains, significant cycle-to-cycle chemical variations occur when

$$\zeta > 1.3 \times 10^{-17} s^{-1} \left( n/2 \times 10^4 cm^{-3} \right).$$

More generally, this is when

$$t_{\rm impact} < 10^{11} s. \left( 6 \times 10^6 cm^{-3}/n \right).$$

In these circumstances, which are not expected to be unusual in star-forming cores, two results follow: (a) the abundances (e.g. of $H_2O$ and CO) may be very significantly enhanced with highly non-linear $\zeta$-dependences, and (b) the chemical evolution of many species (e.g. $NH_3$) will occur over many cycles and the time-scale for the changes will be significantly larger than that for either the freeze-out of gas-phase species, or the interval between cosmic ray impacts. Obviously, in these conditions, the continuous desorption simplification is not applicable. Recent studies, which include a spectrum of cosmic ray energies and therefore a range of values of $t_{\rm impact}$, indicate that these effects cannot be ignored.

(vi) Whether or not different ice components can co-desorb - where the desorption characteristics of one species affects others – is somewhat speculative and will be strongly dependent on the compositional structure of the ices. However, the presence of even limited levels of species co-desorption results in very large ($\gtrsim$10–100 ×) enhancements of the effective desorption rates and predicted gas-phase abundances (especially for densities $\gtrsim 10^5$ cm$^{-3}$).

(vii) Similar, but more species-specific, enhancements are obtained if a population of very small grains exist, from which complete ice mantle sublimation is possible following each cosmic ray heating event. Here, the strongest enhancements are for the more tightly bound species, so that a chemical signature of the presence of these grains may be detectable. Generally, if either co-desorption occurs and/or very small grains can survive to high densities, then the desorption rates from tightly bound species (such as $H_2O$) would be very strongly enhanced.

(viii) At extinctions $A_{\rm v} \gtrsim 5.5$, which applies throughout most of the gas in dense star-forming cores, photodesorption is dominated by the cosmic ray induced radiation field. The photodesorption rates (cm$^{-3}$ s$^{-1}$) are given by $\dot{n}_{\rm i} = Y_{\rm i} F_{\rm cr} \sigma_{\rm H} n_{\rm H} f_{\rm i}$ where $Y_{\rm i} \sim 10^{-3}$ is the photodesorption yield and $F_{\rm cr}$ is the cosmic ray induced photon flux (typically ∼5000 photons cm$^{-2}$ s$^{-1}$). Comparing this to the desorption rate for cosmic ray heating (equation 3), we can see that (noting that both processes scale with $\zeta$) desorption by cosmic ray heating dominates over photodesorption when

$$k^{\rm i}_{\rm crd} > \frac{Y_{\rm i} F_{\rm cr}}{N_{\rm s}} \sim 5 \times 10^{-15} s^{-1}.$$

Comparing this to the values given in Tables 3, 4, and 5 we can conclude that (even without the additional enhancements to the rates due to sporadic heating, co-desorption or the presence of small grains) cosmic ray heating will dominate over photodesorption for most species in dense, dark environments. This is an important result that is in direct contrast to the findings of previous studies (e.g. Shen et al. 2004) and is a consequence of the higher values that we have determined for the cosmic ray induced desorption rates. To illustrate this point, we have re-run several of the models including the full range of desorption mechanisms (direct and cosmic ray-induced photodesorption, enthalpy of formation/$H_2$ formation driven desorption etc.) and a limited surface chemistry. This model is therefore closer to that which might be used to simulate real molecular clouds/star-forming regions. The results, for selected species, are shown in Table 11. This table also includes results from a reference model (as Model 1, but without any cosmic ray desorption) for comparison.

These results clearly show the significance of cosmic ray induced desorption, with the abundances of many species showing dramatic differences relative to the reference model. Whilst the effects on more tightly bound species, such as $H_2O$ and $CO_2$, are more marginal these are also dramatically enhanced if co-desorption occurs.

The significance of these results is most apparent in the dense, dark regions whose chemistry and dynamics are used to diagnose the physics of the early stages of star formation, and which may form the chemical 'legacy' to protoplanetary discs.

Finally, we note that there are additional implications of the cosmic ray interactions that we have not considered in this study, such as the effects on the grain charge (Ivlev et al. 2015b) or the cosmic ray driven non-thermal chemistry within the ices (Silsbee et al. 2021). In future work, we will assess the importance of the updates that we have discussed in this study in realistic astrochemical models of specific sources. To do that we will also consider the application to a range of grain sizes and (possibly attenuated) cosmic ray energy spectra, whilst being mindful of the many uncertainties that exist.

## ACKNOWLEDGEMENTS

The author thanks the anonymous referee for helpful comments and suggestions that have improved this paper.

## DATA AVAILABILITY

The data underlying this study are openly available from the published papers that are cited in the article. No new data were generated in support of this research.

## REFERENCES


Bringa E. M., Johnson R. E., 2004, ApJ, 603, 159
Caselli P. et al., 2012, ApJ, 759, L37
Cecchi– Pestellini C., Rawlings J. M. C., Viti S., Williams D. A., 2010, ApJ, 725, 1581
Cernicharo J., Marcelino J., Roueff E., Gerin M., Jiménez-Escobar A., Muñoz Caro G. M., 2012, ApJ, 759, L43
Collings M. P. et al., 2004, MNRAS, 354, 1133
Collings M. P., Frankland V., Lasne J., Marchione D., Rsu-Finsen A., McCoustra M. R. S., 2015, MNRAS, 449, 1826
d'Hendecourt L. B., Allamandola L. J., Baas F., Greenberg J. M., 1982, A&A, 109, L12
Hasegawa T. I., Herbst E., 1993, MNRAS, 261, 83 (HH93)
Herbst E., Cuppen H. M., 2006, Proc. Natl. Acad. Sci., 103, 12257
Ivlev A. V., Röcker T. B., Vasyunin A., Caselli P., 2015, ApJ, 805, 59
Ivlev A. V., Padovani M., Galli D., Caselli P., 2015, ApJ, 812, 135
Kalvāns J., 2016, ApJS, 224, 42
Kalvāns J., 2021, ApJ, 910, 54
Kalvāns J., Kalnin J. R., 2019, MNRAS, 486, 2050
Kalvāns J., Kalnin J. R., 2020a, A&A, 633, A97
Kalvāns J., Kalnin J. R., 2020b, A&A, 641, A49
Léger A., Jura M., Omont A., 1985, A&A, 144, 147
Mathis J. S., Rumpl W., Nordsieck K. H., 1977, ApJ, 217, 425
Minissale M., Dulieu F., Cazaux S., Hocuk S., 2016, A&A, 585, A24
Öberg K. I., van Broekhuizen F., Fraser H. J., Bisschop S. E., van Dishoeck E. F., Schlemmer S., 2005, ApJ, 621, L33
Öberg K. I., Linnartz H., Visser R., van Dishoeck E. F., 2009, ApJ, 693, 1209
Öberg K. I., van Dishoeck E. F., Linnartz H., 2009, A&A, 496, 281
Prasad S. S., Tarafdar S. P., 1983, ApJ, 267, 603
Rawlings J. M. C., Williams D. A., 2021, MNRAS, 500, 5117
Rawlings J. M. C., Williams D. A., Viti S., Cecchi-Pestellini C., Duley W. W., 2013, MNRAS, 430, 264
Roberts J. F., Rawlings J. M. C., Viti S., Williams D. A., 2007, MNRAS, 382, 733
Schutte W. A., Greenberg J. M., 1991, A&A, 244, 190
Shen C. J., Greenberg J. M., Schutte W. A., van Dishoeck E. F., 2004, A&A, 415, 203
Shingledecker C. N., Tennis J., Le Gal R., Herbst E., 2018, ApJ, 861, 20
Silsbee K., Caselli P., Ivlev A. V., 2021, MNRAS, 507, 6205
Sipilä O., Zhao B., Caselli P., 2020, A&A, 640, A94
Sipilä O., Silsbee K., Caselli P., 2021, ApJ, 922, 126
Tafalla M., Myers P. C., Caselli P., Walmsley C. M., 2004, A&A, 416, 191
van Dishoeck E. F. et al., 2021, A&A, 648, 24
Viti S., Collings M. P., Dever J. W., McCoustra M. R. S., Williams D. A., 2004, MNRAS, 354, 1141
Watson W. D., 1976, Rev. Mod. Phys., 48, 513
Zhao B., Caselli P., Li Z-Y., 2018, MNRAS, 478, 2723


This paper has been typeset from a TEX/LATEX file prepared by the author.